

Neutron stars with a generalized Proca hair and spontaneous vectorization

Ryotaro Kase¹, Masato Minamitsuji², and Shinji Tsujikawa¹

¹*Department of Physics, Faculty of Science, Tokyo University of Science,
1-3, Kagurazaka, Shinjuku-ku, Tokyo 162-8601, Japan*

²*Centro Multidisciplinar de Astrofísica - CENTRA, Departamento de Física,
Instituto Superior Técnico - IST, Universidade de Lisboa - UL,
Avenida Rovisco Pais 1, 1049-001 Lisboa, Portugal*

(Dated: July 28, 2020)

In a class of generalized Proca theories, we study the existence of neutron star solutions with a nonvanishing temporal component of the vector field A_μ approaching 0 toward spatial infinity, as they may be the endpoints of tachyonic instabilities of neutron star solutions in general relativity with $A_\mu = 0$. Such a phenomenon is called spontaneous vectorization, which is analogous to spontaneous scalarization in scalar-tensor theories with nonminimal couplings to the curvature or matter. For the nonminimal coupling βXR , where β is a coupling constant and $X = -A_\mu A^\mu/2$, we show that there exist both 0-node and 1-node vector-field solutions, irrespective of the choice of the equations of state of nuclear matter. The 0-node solution, which is present only for $\beta = -\mathcal{O}(0.1)$, may be induced by some nonlinear effects such as the selected choice of initial conditions. The 1-node solution exists for $\beta = -\mathcal{O}(1)$, which suddenly emerges above a critical central density of star and approaches the general relativistic branch with the increasing central density. We compute the mass M and radius r_s of neutron stars for some realistic equations of state and show that the M - r_s relations of 0-node and 1-node solutions exhibit notable difference from those of scalarized solutions in scalar-tensor theories. Finally, we discuss the possible endpoints of tachyonic instabilities.

I. INTRODUCTION

The advent of gravitational-wave (GW) astronomy [1], along with observations of binary pulsars [2], opened up a new channel for probing physics of high-density matter inside neutron stars (NSs). In terms of the tidal deformability of NSs, the data of the GW170817 event [3] put constraints on the relation between mass and radius of NSs. In addition, the recent X-ray data collected by NASA's *NICER* mission [4] inferred mass and radius of a millisecond pulsar as well as equation of state (EOS) [5]. With the accumulation of GW and other events in the future along with the increasing accuracy of measurements, we will be able to place tighter bounds on NS EOSs as well as the possible deviation from General Relativity (GR) in high-density regions. In particular, whether or not some extra degrees of freedom beyond GR and standard model of particle physics exist around strong gravitational objects is an important question. Moreover, such new degrees of freedom may be related to the problems of dark sectors in our Universe such as dark matter and dark energy (see, e.g., Ref. [6] for the observational constraint on dark energy models from GW170817 event).

One of the simplest and well-motivated modifications to GR in the regime of strong gravity is to introduce nonlinear scalar curvature terms like R^2 in the Lagrangian, besides the Einstein-Hilbert term R [7]. This theory, which is known as a class of $f(R)$ gravity [8, 9], has one additional scalar degree of freedom in comparison to GR, with an effective potential arising from the gravitational origin [10]. NS solutions in $f(R)$ gravity have been extensively studied in the literature [11–16], but the presence of nonvanishing scalar mass can give rise to an exponential growing mode outside the star [17]. This is the case for the model $f(R) = R + \alpha R^2$ with α being constant, in which the scalar degree of freedom does not vanish at spatial infinity unless EOS inside NSs is chosen in a specific way [18].

One can express $f(R)$ theories in terms of the action of scalar-tensor theories with a nonminimal coupling to the Ricci scalar. There are also other scalar-tensor theories in which a scalar field ϕ is nonminimally coupled to the Ricci scalar R of the form $F(\phi)R$, where $F(\phi)$ is a function of ϕ [19, 20]. For the massless scalar field in Brans-Dicke theories with the coupling $F(\phi) = e^{-2Q\phi/M_{\text{pl}}}$ [19], where Q is a constant and M_{pl} is the reduced Planck mass, it is possible to realize a nontrivial configuration of the field inside NS with ϕ approaching 0 at spatial infinity [17]. In scalar-tensor theories, the construction of hairy solutions in compact objects and their observational signatures have been studied in Refs. [21–23].

While the theory with a monotonic coupling function $F(\phi)$ only admits NS solutions with a nontrivial profile of ϕ , a theory with $F_{,\phi}(0) = 0$, where $F_{,\phi} = dF/d\phi$, also admits NS solutions in GR with $\phi = 0$. The effective mass squared for small perturbations about the GR NS solution is given by $m_{\text{eff}}^2 = -(M_{\text{pl}}^2/2)[F_{,\phi\phi}(0)/\omega(0)]R$, see Eq. (A.1) in Appendix for our convention. Provided that $F_{,\phi\phi}(0) > 0$ with $R > 0$ and $\omega(0) > 0$, there is a tachyonic instability of the GR branch, which can be triggered by spontaneous growth of ϕ toward the other nontrivial branch. Then, NSs may eventually acquire a scalar hair, whose phenomenon is dubbed *spontaneous scalarization*. Spontaneous scalarization is particularly interesting, as it would modify the gravitational interaction only in strong-gravity regimes

and be directly tested via future GW measurements.

Damour and Esposito-Farese [24, 25] proposed a concrete nonminimal coupling $F(\phi) = e^{-\beta\phi^2/(2M_{\text{pl}}^2)}$ for spontaneous scalarization, which satisfies the conditions $F_{,\phi}(0) = 0$ and $F_{,\phi\phi}(0) > 0$ for $\beta < 0$. They showed that there exist the spherically symmetric and static NS solutions with a nonvanishing field configuration besides the GR branch. In Refs. [26–28], it was shown that the GR solution can be unstable to trigger spontaneous scalarization to the other nontrivial branch for $\beta < -4.35$, depending very weakly on the choice of EOSs. Since the scalarized solution has a scalar charge associated with the energy loss through dipolar radiation, binary-pulsar observations have placed the bound $\beta > -4.5$ [29] (see also Refs. [30–32]). These two results confine the coupling β to a limited range. On the other hand, it has been shown that spontaneous scalarization can also be realized for black holes, in the presence of couplings to the Gauss-Bonnet term [33–39] and to the electromagnetic field [40–44]. The threshold values of generalized scalar-tensor couplings for the tachyonic instability and the onset of spontaneous scalarization have been extensively studied in Ref. [45].

The nonminimally coupled scalar field is not only the possibility for modifying the physical property of NSs, but the vector field A_μ coupled to gravity should also affect the structure of NSs. Thus, in analogy to spontaneous scalarization, it is of interest to study the possibility of *spontaneous vectorization* in vector-tensor theories. The standard Einstein-Maxwell theory is given by the Lagrangian $L = M_{\text{pl}}^2 R/2 - F_{\mu\nu}F^{\mu\nu}/4$, where $F_{\mu\nu} = \nabla_\mu A_\nu - \nabla_\nu A_\mu$ is the Maxwell tensor with ∇_μ being the covariant derivative operator. The simple example for modifying the gravitational interaction in GR is to introduce the nonminimal coupling $G_4(X)R$, where G_4 is a function of $X = -A^\mu A_\mu/2$. In this Hellings and Nordtvedt theory [46], Annulli *et al.* [47] found NS solutions with a nonvanishing temporal vector component approaching 0 at spatial infinity, besides the GR branch. The possibility of spontaneous vectorization was analyzed from the viewpoint of Einstein frame in Refs. [48, 49].

The vector-tensor theories with the coupling $G_4(X)R$ alone generally give rise to derivatives higher than second order in the field equations of motion, so it can be prone to the problem of Ostrogradski instabilities [50, 51] with the Hamiltonian unbounded from below. The theories remain up to second order by taking into account additional derivative-interaction terms to the Lagrangian of the form $G_{4,X}(X)[(\nabla_\mu A^\mu)^2 - \nabla_\mu A_\nu \nabla^\nu A^\mu]$, where $G_{4,X} \equiv dG_4/dX$. They are known as a class of generalized Proca (GP) theories [52–55], in which the $U(1)$ gauge symmetry is broken by the explicit X dependence in G_4 . The application of GP theories to the late-time cosmic acceleration [56–59] and the screening of fifth forces [60, 61] around local objects on the weak gravitational background has been widely studied in the literature.

If we apply GP theories to compact objects on the strong gravitational background, there are hairy NS and black hole solutions with nontrivial vector-field profiles [62–70]. In Refs. [63, 70], NS solutions were studied for polytropic EOS for the models which only have hairy NS solutions. Models associated with spontaneous vectorization should possess a nonvanishing vector field with A_μ approaching 0 at spatial infinity, which hence would arise from a tachyonic instability of the GR solution with $A_\mu = 0$. For the former branch, there will be a nontrivial modification to the structure of NSs (like mass and radius) with A_μ carrying a vector charge.

In this paper, we study NS solutions in the above class of GP theories with the nonvanishing vector-field profile approaching 0 far outside the star. To describe realistic nuclear interactions inside NSs, we use the analytic representations of SLy and BSk20 EOSs given in Refs. [71, 72]. We consider the simple nonminimal coupling βX in $G_4(X)$, which allows for nontrivial vector-field solutions besides the GR branch. We will show that there are either 0-node or 1-node solutions depending on whether the coupling β is of order -0.1 or -1 , respectively. The 0-node solution in GP theories has a different property compared to that in scalar-tensor theories, in that the former may appear through some nonlinear effects like the selected choice of initial conditions. We will also show that the value of β for the 1-node solution is consistent with the onset of instability. We will compute the mass and radius of NSs for both 0-node and 1-node solutions and investigate how they are modified from those in GR. Finally, we will clarify the difference from the case of scalarized solutions and discuss the possible endpoints of tachyonic instabilities.

Throughout the paper, we use the natural units $c = \hbar = 1$, where c is the speed of light and \hbar is reduced Planck constant. When these fundamental constants are needed in numerical computations, we recover them and adopt their concrete values $c = 2.9979 \times 10^{10} \text{ cm} \cdot \text{s}^{-1}$ and $\hbar = 1.0546 \times 10^{-27} \text{ erg} \cdot \text{s}$, and the Newton gravitational constant $G = 6.6743 \times 10^{-8} \text{ g}^{-1} \cdot \text{cm}^3 \cdot \text{s}^{-2}$. In terms of the normalization of vector field, it is convenient to use the reduced Planck mass M_{pl} , which is related to G as $M_{\text{pl}} = (8\pi G)^{-1/2}$.

II. GENERALIZED PROCA THEORIES AND RELATIVISTIC STARS

We consider a vector field A_μ breaking the $U(1)$ gauge symmetry due to the presence of nonminimal coupling $G_4(X)R$, where X is a function of $X = -A^\mu A_\mu/2$ and R is the Ricci scalar. This type of nonminimal vector coupling to gravity was first introduced by Hellings and Nordtvedt in 1973 [46], but we need to worry for Ostrogradski instabilities associated with the existence of derivatives higher than second order. The theory can be made second

order by adding a counter term that eliminates higher-order derivatives. The action of such second-order GP theories is given by [52–55]

$$\mathcal{S} = \int d^4x \sqrt{-g} \left[G_4(X)R + G_{4,X}(X) \{ (\nabla_\mu A^\mu)^2 - \nabla_\mu A_\nu \nabla^\nu A^\mu \} - \frac{1}{4} F_{\mu\nu} F^{\mu\nu} \right] + \mathcal{S}_m(g_{\mu\nu}, \Psi_m), \quad (2.1)$$

where g is the determinant of metric tensor. We take into account the action \mathcal{S}_m of matter fields Ψ_m , which are assumed to be minimally coupled to gravity. The action (2.1) can be generalized further to include other derivative and nonminimal couplings [52–55, 73, 74], but we will focus on the theory (2.1) for simplicity.

A. Background equations

The line element on a spherically symmetric and static background is given by

$$ds^2 = -f(r)dt^2 + h^{-1}(r)dr^2 + r^2 (d\theta^2 + \sin^2\theta d\varphi^2), \quad (2.2)$$

where f and h are functions of the radial coordinate r from the center of symmetry. On this background, the vector field is expressed in the form

$$A_\mu = (A_0(r), A_1(r), 0, 0), \quad (2.3)$$

where $A_0(r)$ and $A_1(r)$ correspond to temporal and radial components, respectively, which depend on r alone. Then, the quantity X is expressed as

$$X = \frac{A_0^2}{2f} - \frac{hA_1^2}{2}. \quad (2.4)$$

For the matter sector, we consider a single perfect fluid whose mixed energy-momentum tensor is given by $T_\nu^\mu = \text{diag}(-\rho(r), P(r), P(r), P(r))$, where $\rho(r)$ and $P(r)$ are the density and pressure, respectively. From the matter continuity equation $\nabla_\mu T_\nu^\mu = 0$, we obtain

$$P' + \frac{f'}{2f}(\rho + P) = 0, \quad (2.5)$$

where a prime represents a derivative with respect to r .

Variation of the action (2.1) with respect to A_1 leads to

$$A_1 [(f - fh - rhf') fG_{4,X} + \{ fh(rf' + f)A_1^2 - rA_0(A_0f' - 2fA_0') \} hG_{4,XX}] = 0. \quad (2.6)$$

This shows that there exists the branch satisfying

$$A_1 = 0. \quad (2.7)$$

Throughout this paper, we will focus on this branch. The difference from the solution in GR arises from the temporal component A_0 . Varying the action (2.1) with respect to f , h , and A_0 , it follows that

$$h' = \frac{4(1-h)(G_4f - A_0^2G_{4,X}) - 2\rho r^2f - r^2hA_0'^2}{4r(G_4f - A_0^2G_{4,X})}, \quad (2.8)$$

$$f' = \frac{f[4f(1-h)G_4 + 2Pr^2f - rhA_0'(rA_0' + 8A_0G_{4,X})]}{4rh(G_4f - A_0^2G_{4,X})}, \quad (2.9)$$

$$A_0'' + \left(\frac{2}{r} - \frac{f'}{2f} + \frac{h'}{2h} \right) A_0' + \frac{2}{r^2h} G_{4,X} (rh' + h - 1) A_0 = 0. \quad (2.10)$$

Substituting Eq. (2.8) into Eq. (2.10), the temporal vector component obeys

$$A_0'' + \left(\frac{2}{r} - \frac{f'}{2f} + \frac{h'}{2h} \right) A_0' - \frac{G_{4,X}(2f\rho + hA_0'^2)}{2h(G_4f - A_0^2G_{4,X})} A_0 = 0. \quad (2.11)$$

Provided that EOS $P = P(\rho)$ inside the star is known, we can solve Eq. (2.5) and Eqs. (2.8)-(2.10) for P , h , f , A_0 with a given function $G_4(X)$. In doing so, we need to impose regular boundary conditions at the center of star.

The general relativistic (GR) solution corresponds to the vanishing temporal component, i.e.,

$$\text{GR} : A_0 = 0. \quad (2.12)$$

We also consider a nonvanishing vector-field solution (VS) characterized by a radial-dependent temporal component $A_0(r)$ with the asymptotic behavior $A_0(r) \rightarrow 0$ as $r \rightarrow \infty$, i.e.,

$$\text{VS} : A_0(r) \neq 0, \quad \text{and} \quad A_0(r \rightarrow \infty) = 0. \quad (2.13)$$

A simple model which may allow for the existence of both (2.12) and (2.13) is given by $G_{4,X} = \beta = \text{constant}$, i.e.,

$$G_4(X) = \frac{M_{\text{pl}}^2}{2} + \beta X, \quad (2.14)$$

where the first term on the right hand side corresponds to the Einstein-Hilbert term. We can also think of other couplings including nonlinear terms of X like $G_4(X) = M_{\text{pl}}^2/2 + \sum_{n=1} \beta_n X^n$, for instance $G_4(X) = (M_{\text{pl}}^2/2)e^{2\beta X/M_{\text{pl}}^2}$, but we will focus on the model (2.14) in this paper. Note that if the linear term of X in $G_4(X)$ is absent, there may not be VS solutions, as in this case the GR branch is expected to be linearly stable and they may be formed from other initial conditions.

B. Boundary conditions

Let us derive general boundary conditions of NSs at $r = 0$ and at spatial infinity for the model given by Eq. (2.14). At the center of star, we impose the regular boundary conditions $P'(0) = \rho'(0) = h'(0) = f'(0) = A_0'(0) = 0$. Then, the solutions around $r = 0$ are expressed in the forms,

$$\begin{aligned} P(r) &= p_c + \sum_{i=2}^{\infty} p_i r^i, & \rho(r) &= \rho_c + \sum_{i=2}^{\infty} \rho_i r^i, \\ h(r) &= 1 + \sum_{i=2}^{\infty} h_i r^i, & f(r) &= f_0 + \sum_{i=2}^{\infty} f_i r^i, & A_0(r) &= A_c + \sum_{i=2}^{\infty} \alpha_i r^i, \end{aligned} \quad (2.15)$$

where $p_c, p_i, \rho_c, \rho_i, h_i, f_0, f_i, A_c, \alpha_i$ are constants. Substituting Eq. (2.15) into Eq. (2.5) and Eqs. (2.8)-(2.10), the iterative solutions around $r = 0$ are given by

$$P(r) = P_c - \frac{f_0(\rho_c + P_c)[\rho_c(f_0 M_{\text{pl}}^2 + \beta A_c^2 - 8\beta^2 A_c^2) + 3P_c(f_0 M_{\text{pl}}^2 - \beta A_c^2)]}{12(f_0 M_{\text{pl}}^2 - \beta A_c^2)^2} r^2 + \mathcal{O}(r^4), \quad (2.16)$$

$$h(r) = 1 - \frac{f_0 \rho_c}{3(f_0 M_{\text{pl}}^2 - \beta A_c^2)} r^2 + \mathcal{O}(r^4), \quad (2.17)$$

$$f(r) = f_0 + \frac{f_0^2[\rho_c(f_0 M_{\text{pl}}^2 + \beta A_c^2 - 8\beta^2 A_c^2) + 3P_c(f_0 M_{\text{pl}}^2 - \beta A_c^2)]}{6(f_0 M_{\text{pl}}^2 - \beta A_c^2)^2} r^2 + \mathcal{O}(r^4), \quad (2.18)$$

$$A_0(r) = A_c + \frac{A_c \beta f_0 \rho_c}{3(f_0 M_{\text{pl}}^2 - \beta A_c^2)} r^2 + \mathcal{O}(r^4). \quad (2.19)$$

We consider a NS with the radius r_s determined by the condition

$$P(r_s) = 0. \quad (2.20)$$

Outside the star ($r > r_s$), both $P(r)$ and $\rho(r)$ vanish. The boundary conditions at spatial infinity are

$$h(r \rightarrow \infty) = 1, \quad f(r \rightarrow \infty) = 1, \quad A_0(r \rightarrow \infty) = 0. \quad (2.21)$$

Under the time reparametrization in the metric (2.2), the asymptotic value of f can be chosen as an arbitrary constant. After performing the replacements $A_c = \sqrt{f_0} \bar{A}_c$, $A_0(r) = \sqrt{f_0} \bar{A}_0(r)$, and $f(r) = f_0 \bar{f}(r)$ in Eqs. (2.16)-(2.19), the constant f_0 disappears in the expressions of $P(r)$, $h(r)$, $\bar{f}(r)$, and $\bar{A}_0(r)$. In other words, we can choose $f_0 = 1$ without loss of generality.

The mass function $\mathcal{M}(r)$ is defined by

$$h(r) = 1 - \frac{2G\mathcal{M}(r)}{r}. \quad (2.22)$$

The Arnowitt-Deser-Misner (ADM) mass is given by the asymptotic value of $\mathcal{M}(r)$ at spatial infinity, i.e.,

$$M \equiv \lim_{r \rightarrow \infty} \mathcal{M}(r) = \frac{r}{2G} [1 - h(r)] \Big|_{r \rightarrow \infty}. \quad (2.23)$$

We introduce the compactness of star, as

$$\mathcal{C} = \frac{GM}{r_s}, \quad (2.24)$$

where G is the Newton gravitational constant. For a given EOS, the radius and mass of a NS are known by numerically integrating Eqs. (2.5) and (2.8)-(2.10) with the boundary conditions (2.16)-(2.19) at $r = 0$. Because of the reflection symmetry under $A_\mu \rightarrow -A_\mu$, we assume that $A_0 \geq 0$ in the rest of paper without loss of generality. Note that we can go back to the conventional units with G and c by the replacement of $M_{\text{pl}} \rightarrow c^2/\sqrt{8\pi G}$ and $\rho \rightarrow \rho c^2$ in the above equations.

C. Equations of state of NSs

As an EOS of relativistic stars, we first discuss the case of constant density ρ in Sec. III. Then, in Secs. IV and V, we will proceed to the analysis of NS structures with a nonvanishing VS for two more realistic EOSs: SLy and BSk20. For the latter EOSs, we introduce the dimensionless quantities,

$$\xi \equiv \log_{10}(\rho/\text{g} \cdot \text{cm}^{-3}) = \alpha_1 + \alpha_2 \ln y, \quad (2.25)$$

$$\zeta \equiv \log_{10}(P/\text{dyn} \cdot \text{cm}^{-2}) = \alpha_3 + \alpha_2 \ln z, \quad (2.26)$$

where $\alpha_1 = \ln(\rho_0/\text{g} \cdot \text{cm}^{-3})/\ln 10$, $\alpha_2 = (\ln 10)^{-1}$, $\alpha_3 = \ln(\rho_0 c^2/\text{dyn} \cdot \text{cm}^{-2})/\ln 10$, and

$$y \equiv \frac{\rho}{\rho_0}, \quad z \equiv \frac{P}{\rho_0}. \quad (2.27)$$

Here, ρ_0 is the density defined by

$$\rho_0 \equiv m_n n_0 = 1.6749 \times 10^{14} \text{ g} \cdot \text{cm}^{-3}, \quad (2.28)$$

where $m_n = 1.6749 \times 10^{-24} \text{ g}$ is the neutron mass and $n_0 = 0.1 \text{ (fm)}^{-3}$ is the typical number density of NSs. SLy and BSk20 EOSs are parameterized as

$$\begin{aligned} \zeta(\xi) = & \frac{a_1 + a_2 \xi + a_3 \xi^3}{1 + a_4 \xi} \{ \exp[a_5(\xi - a_6)] + 1 \}^{-1} + (a_7 + a_8 \xi) \{ \exp[a_9(a_{10} - \xi)] + 1 \}^{-1} \\ & + (a_{11} + a_{12} \xi) \{ \exp[a_{13}(a_{14} - \xi)] + 1 \}^{-1} + (a_{15} + a_{16} \xi) \{ \exp[a_{17}(a_{18} - \xi)] + 1 \}^{-1} \\ & + \frac{a_{19}}{1 + [a_{20}(\xi - a_{21})]^2} + \frac{a_{22}}{1 + [a_{23}(\xi - a_{24})]^2}. \end{aligned} \quad (2.29)$$

For SLy, the coefficients a_1, \dots, a_{18} are given in Table 1 of Ref. [71], with $a_{19} = a_{20} = a_{21} = a_{22} = a_{23} = a_{24} = 0$. For BSk20, the coefficients are presented in Ref. [72] with the correspondence $a_i = \bar{a}_i$ for $1 \leq i \leq 9$, $a_{10} = \bar{a}_6$ and $a_i = \bar{a}_{i-1}$ for $11 \leq i \leq 24$, where \bar{a}_i are the values given in the center of Table 2 in Ref. [72].

III. RELATIVISTIC STARS WITH CONSTANT DENSITY

In this section, we consider relativistic stars with the constant density ρ_c to understand properties of the nonvanishing VS analytically.

In the absence of the vector field A_μ , there exist analytic solutions to Eqs. (2.5), (2.8), and (2.9). The metric components inside the star ($r \leq r_s$) are given by

$$f = \left[\frac{3}{2} \sqrt{1 - 2\mathcal{C}} - \frac{1}{2} \sqrt{1 - 2\mathcal{C} \frac{r^2}{r_s^2}} \right]^2, \quad h = 1 - 2\mathcal{C} \frac{r^2}{r_s^2}, \quad (3.1)$$

with

$$\frac{P}{\rho_c} = \frac{\sqrt{1 - 2\mathcal{C} r^2/r_s^2} - \sqrt{1 - 2\mathcal{C}}}{3\sqrt{1 - 2\mathcal{C}} - \sqrt{1 - 2\mathcal{C} r^2/r_s^2}}, \quad \mathcal{C} = \frac{\rho_c r_s^2}{6M_{\text{pl}}^2}. \quad (3.2)$$

The geometry outside the star ($r > r_s$) is described by the Schwarzschild metric,

$$f = h = 1 - 2\mathcal{C} \frac{r_s}{r}. \quad (3.3)$$

From $r = 0$ to $r = r_s$, the function f increases from $(3\sqrt{1 - 2\mathcal{C}} - 1)^2/4$ to $1 - 2\mathcal{C}$. This increase of f leads to the decrease of P as a function of r according to Eq. (2.5). The stellar radius r_s is determined by the point at which P vanishes. From Eqs. (3.1) and (3.3), the function h reaches a minimum at $r = r_s$ and it starts to grow for $r > r_s$.

As we observe in Eqs. (2.8) and (2.9), the existence of nonvanishing A_0 affects the metric components h and f , so that Eqs. (3.1) and (3.3) are subject to modifications. Before addressing this point, we first derive analytic solutions to $A_0(r)$ under some approximations to extract general properties of nonvanishing VSs. We then study the full numerical solution to $A_0(r)$ and discuss its effect on the metrics.

A. Approximate vector-field solutions in the weak gravitational background

In the presence of A_μ , the temporal vector component inside the star obeys

$$A_0'' + \left(\frac{2}{r} - \frac{f'}{2f} + \frac{h'}{2h} \right) A_0' - \frac{\beta(2f\rho_c + hA_0'^2)}{h(fM_{\text{pl}}^2 - \beta A_0^2)} A_0 = 0, \quad (3.4)$$

which allows the existence of the GR branch (2.12). To discuss whether the GR solution can be unstable to reach a VS with nonvanishing A_0 , we take into account the perturbation $\delta A_0(r)$ around $A_0 = 0$. Then, $\delta A_0(r)$ has the negative mass squared $m_{\text{eff}}^2 = 2\beta\rho_c/M_{\text{pl}}^2$ for

$$\beta < 0, \quad (3.5)$$

which is at least necessary for spontaneous vectorization to occur.

If we consider the weak gravitational background with $\mathcal{C} \ll 1$, the following two conditions are satisfied,

$$\frac{1}{r} \gg \left\{ \left| \frac{f'}{f} \right|, \left| \frac{h'}{h} \right| \right\}, \quad |h - 1| \ll 1. \quad (3.6)$$

In realistic NSs the conditions (3.6) can be violated, but we will temporarily use them for the purpose of deriving analytic solutions approximately. Let us also discuss the case in which $A_0'^2$ and A_0^2 are in the ranges,

$$f\rho_c \gg hA_0'^2, \quad fM_{\text{pl}}^2 \gg |\beta|A_0^2. \quad (3.7)$$

Under the conditions (3.6) and (3.7), Eq. (3.4) is approximately given by

$$A_0'' + \frac{2}{r} A_0' - \frac{12\beta\mathcal{C}}{r_s^2} A_0 \simeq 0. \quad (3.8)$$

Let us derive the solution to Eq. (3.8) for $\beta < 0$. Imposing the boundary conditions $A_0(r = 0) = A_c = \text{constant}$ and $A_0'(r = 0) = 0$ at the center, the resulting internal solution (for $r \leq r_s$) is

$$A_0(r) \simeq A_c \frac{\sin(br/r_s)}{br/r_s}, \quad (3.9)$$

where

$$b \equiv \sqrt{-12\beta\mathcal{C}}. \quad (3.10)$$

Outside the star the density ρ_c vanishes, while $hA_0'^2$ does not, so the first condition of Eq. (3.7) is violated. Dropping the term $hA_0'^2$ for the moment and employing the first condition of Eq. (3.6) outside the star, Eq. (3.4) approximately reduces to

$$A_0'' + \frac{2}{r}A_0' \simeq 0. \quad (3.11)$$

In this case, the external solution reads

$$A_0(r) \simeq A_\infty + \frac{Q}{r}, \quad (3.12)$$

where A_∞ and Q are constants. Matching the two solutions (3.9) and (3.12), and their first derivatives, respectively at $r = r_s$, we obtain the following two relations,

$$\frac{A_c}{A_\infty} \simeq \frac{1}{\cos b}, \quad \frac{Q}{A_c r_s} \simeq \frac{\sin b}{b} - \cos b. \quad (3.13)$$

For $b \simeq \pi/2 - 0$, there exists the VS with $A_\infty \simeq +0$ and the positive charge $Q = (2/\pi)A_c r_s$. From Eq. (3.9), we have $A_0(r) = (2/\pi)A_c$ at $r = r_s$. In this case, the temporal vector component monotonically decreases toward the asymptotic value $A_\infty \simeq 0$ without crossing $A_0(r) = 0$. This VS is called the *0-node* solution. Under the above approximation scheme, the criterion for the existence of 0-node solutions is that β is smaller than the critical value β_c satisfying $b = \pi/2$, i.e., $\beta < -\pi^2/(48\mathcal{C})$. For NSs with $\mathcal{C} = 0.2$, this condition translates to $\beta < -1$.

For $b \simeq 3\pi/2 - 0$, we also have the other VS with $A_\infty \simeq -0$ and the negative charge $Q = -(2/3\pi)A_c r_s$. In this case, the VS crosses $A_0(r) = 0$ at $r = 2r_s/3$ inside the star and reaches the negative value $A_0(r) = -2A_c/(3\pi)$ at $r = r_s$. Then, $A_0(r)$ increases according to $A_0(r) \simeq Q/r$ with $Q < 0$ toward the asymptotic value -0 . This VS is called the *1-node* solution, which crosses the point $A_0(r) = 0$ once.

In general, the VS with n nodes corresponds to $b \simeq (2n+1)\pi/2 - 0$ with the charge $Q = (-1)^n(2/\pi)(2n+1)^{-1}A_c r_s$. In this case, the vector field crosses $A_0(r) = 0$ for n times with the asymptotic behavior $A_0(r) \simeq Q/r$ at spatial infinity. For even and odd n , the charge Q is positive and negative, respectively.

B. Full vector-field solutions

The relations (3.13) have been derived by exploiting the conditions (3.6) and (3.7) to Eq. (3.4). However, these conditions can be violated for realistic NSs with $\mathcal{C} = \mathcal{O}(0.1)$. If we use the Schwarzschild interior solution (3.1) to estimate the term in front of A_0' in Eq. (3.4), it follows that

$$\frac{2}{r} - \frac{f'}{2f} + \frac{h'}{2h} \simeq \frac{2}{r} \left[1 - \mathcal{O}(1)\mathcal{C}\frac{r^2}{r_s^2} \right]. \quad (3.14)$$

As we will see later, the metric functions f and h are subject to modifications by the backreaction of A_0 . Still, the estimation (3.14) is sufficient for the purpose of understanding the metric corrections to the leading-order term $2/r$. From Eq. (3.14), the compactness \mathcal{C} of order 0.1 works to reduce the friction term in Eq. (3.4), whose effect is particularly strong around $r = r_s$. The metric component h , which appears in the denominator of the third term on the left hand side of Eq. (3.4), reaches a minimum value $1 - \mathcal{O}(1)\mathcal{C}$ around $r = r_s$. These properties show that, in comparison to the weak gravitational background with \mathcal{C} much smaller than 0.1, the decrease of $A_0(r)$ inside the star is faster than that estimated by Eq. (3.9). In other words, when $\beta = -\mathcal{O}(1)$, the solutions can enter the negative $A_0(r)$ region, in which case the 0-node solution can disappear. Instead, it may be possible to realize the 1-node solution even for $\beta = -\mathcal{O}(1)$. It is also expected that the 0-node solution may be present for $|\beta|$ smaller than the order 1.

The field derivative $hA_0'^2$ in Eq. (3.4) leads to the faster decrease of A_0 inside the star as well, whose effect is largest around $r = r_s$. The term $-\beta A_0^2$ gives rise to the contribution to fM_{pl}^2 for $A_0 > \mathcal{O}(0.1)M_{\text{pl}}$, but the modification tends to be unimportant for increasing r due to the decrease of $|A_0(r)|$. We recall that the term $hA_0'^2$ is present even outside the star. Let us estimate the correction induced by this term to the solution (3.12). In doing so, we consider the regime $r \gg r_s$ in which f and h are close to 1 with $fM_{\text{pl}}^2 \gg |\beta|A_0^2$. Then, Eq. (3.4) reduces to

$$A_0'' + \frac{2}{r}A_0' \simeq \frac{\beta}{M_{\text{pl}}^2}A_0'^2 A_0. \quad (3.15)$$

Substituting the leading-order solution (3.12) to the right hand side of Eq. (3.15), we obtain the integrated solution,

$$A_0(r) \simeq \left(1 + \frac{\beta Q^2}{2M_{\text{pl}}^2 r^2}\right) A_\infty + \left(1 + \frac{\beta Q^2}{6M_{\text{pl}}^2 r^2}\right) \frac{Q}{r}. \quad (3.16)$$

The negative coupling β works to suppress the amplitude of $A_0(r)$, but it still has the dependence $A_0(r) \simeq Q/r$ for sufficiently large r . The internal and external solutions of $A_0(r)$ discussed above join each other at $r = r_s$.

In order to confirm the presence of 0-node as well as 1-node solutions, we numerically solve the full background equations with the boundary conditions (2.16)-(2.19) around $r = 0$. For this purpose, we define the dimensionless quantities,

$$m \equiv \frac{3\mathcal{M}}{4\pi\rho_0 r_0^3}, \quad \bar{A}_0 \equiv \frac{A_0}{M_{\text{pl}}}, \quad s \equiv \ln \frac{r}{r_0}, \quad (3.17)$$

where

$$r_0 \equiv \frac{c}{\sqrt{G\rho_0}} = 89.664 \text{ km}. \quad (3.18)$$

On using Eqs. (2.5) and (2.8)-(2.10) with Eq. (2.22), we can derive the differential equations for f , m , \bar{A}_0 , and $z = P/\rho_0$ with respect to the variable s . In this section, we are considering the star with constant $y = \rho/\rho_0$ for $r \leq r_s$.

We find that the 0-node solution is present for

$$-2 \lesssim \beta \lesssim -0.1. \quad (3.19)$$

Thus, there exists the 0-node solution even for $\beta = -\mathcal{O}(0.1)$. The numerical computation also shows the existence of 1-node solutions for

$$\beta \lesssim -2. \quad (3.20)$$

As we discussed above, strong gravitational effects associated with f, h and the existence of term hA_0^2 in Eq. (3.4) lead to the larger effective coupling β , so that the nonvanishing VS tends to enter the negative A_0 region for $\beta = -\mathcal{O}(1)$. For $\beta \lesssim -\mathcal{O}(10)$, we also find the existence of 2-node solutions (and plausibly higher-node solutions), but we will not consider the regime of such large coupling $|\beta|$.

Note that our model corresponds to the special case of $\eta = -2\Omega$ in the notation of Ref. [47], and the correspondence with our notation is $\beta = \Omega/2$. Equation (23) in Ref. [47] shows that under the weak gravitational approximation the tachyonic instability of a GR constant density star in the polar perturbation sector would appear below $\beta \approx -\pi^2/(12\mathcal{C})$, which would be of $\mathcal{O}(-5)$ when extrapolated to the compactness $\mathcal{C} = \mathcal{O}(0.15)$. Thus, the value of β for the 1-node solution is somewhat consistent with that for the critical coupling associated with the onset of tachyonic instability. This motivates us to study the 1-node VS in more details.

In the left panel of Fig. 1, we plot \bar{A}_0 versus r/r_0 corresponding to the 0-node solution for $\beta = -0.4$. In this case, the temporal vector component continuously decreases with the increase of r toward the asymptotic value $A_0 \simeq +0$. We also compute the following dimensionless quantity,

$$\bar{Q} \equiv -\frac{r^2 A_0'}{r_0 M_{\text{pl}}}. \quad (3.21)$$

Provided that A_0 behaves as Eq. (3.16) for $r \gg r_s$, \bar{Q} should approach constant value $Q/(r_0 M_{\text{pl}})$. Indeed, as we see in the left panel of Fig. 1, the numerical value of \bar{Q} approaches a positive constant. This means that the 0-node solution has a positive charge Q with $A_0(r)$ decreasing as $\propto Q/r$ at spatial infinity.

The right panel of Fig. 1 shows \bar{A}_0 and \bar{Q} versus r/r_0 for $\beta = -5$, which corresponds to the 1-node solution. In this case, the stellar radius is $r_s = 0.09r_0$, around which $A_0(r)$ reaches a negative minimum. Outside the star, $A_0(r)$ asymptotically approaches the value -0 with the dependence $A_0(r) \simeq Q/r$. Indeed, the quantity (3.21) approaches a negative constant and hence the 1-node solution has a negative charge Q .

In the following, we estimate the backreaction of vector field on the metric components f and h . We recall that the iterative solutions to P , h , f around $r = 0$ are given by Eqs. (2.16)-(2.18). As long as $f_0 M_{\text{pl}}^2 \gg |\beta| A_c^2$, we have $h \simeq 1 - \rho_c r^2 / (3M_{\text{pl}}^2)$ from Eq. (2.17) and hence h behaves in the same manner as in GR. On the other hand, the r derivative of Eq. (2.18) is given by

$$f'(r) \simeq \frac{f_0^2 [\rho_c (f_0 M_{\text{pl}}^2 + \beta A_c^2 - 8\beta^2 A_c^2) + 3P_c (f_0 M_{\text{pl}}^2 - \beta A_c^2)]}{3(f_0 M_{\text{pl}}^2 - \beta A_c^2)^2} r. \quad (3.22)$$

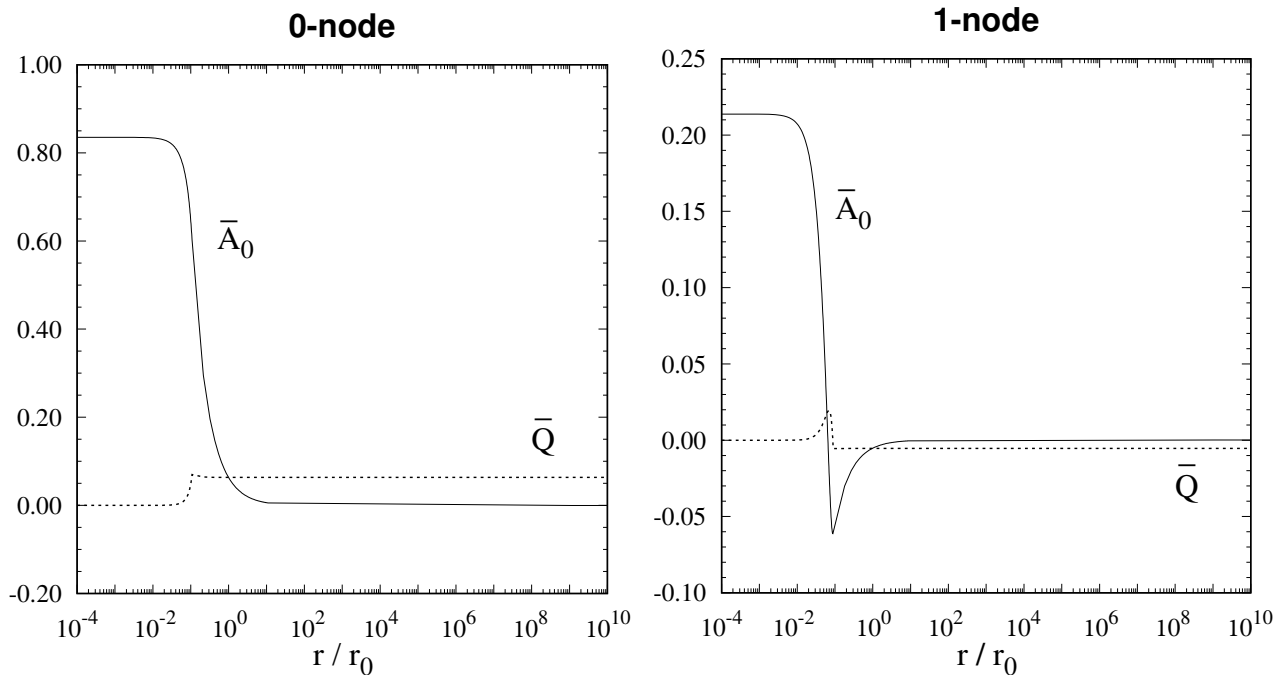


FIG. 1. (Left) Example of the 0-node solution showing $\bar{A}_0 = A_0/M_{\text{pl}}$ and $\bar{Q} = -r^2 A'_0/(r_0 M_{\text{pl}})$ versus r/r_0 for $\beta = -0.4$, $A_c = 0.83525M_{\text{pl}}$, $\rho_c = 7\rho_0$, and $P_c = 0.1946\rho_0$. (Right) Example of the 1-node solution showing $\bar{A}_0 = A_0/M_{\text{pl}}$ and $\bar{Q} = -r^2 A'_0/(r_0 M_{\text{pl}})$ versus r/r_0 for $\beta = -5.0$, $A_c = 0.21377M_{\text{pl}}$, $\rho_c = 9\rho_0$, and $P_c = 0.5640\rho_0$.

The term $-8\beta^2 A_c^2$ is -8β times as large as the term βA_c^2 . This means that, for $\beta < -\mathcal{O}(0.1)$, the former cannot be neglected relative to the latter. Moreover, both $-8\beta^2 A_c^2$ and βA_c^2 work to reduce the derivative $f'(r)$. From Eq. (2.5), this means that the pressure $P(r)$ changes slowly toward the surface of star. In the pressure (2.16) there are also the terms $-8\beta^2 A_c^2$ and βA_c^2 , which prevent the decrease of $P(r)$ induced by the term $f_0 M_{\text{pl}}^2$. In other words, the vector field acts as the repulsive force to gravity. The Schwarzschild internal solutions to f and P , which are given in Eqs. (3.1) and (3.2), are no longer valid for the coupling $\beta < -\mathcal{O}(0.1)$.

The slow change of $P(r)$ for $\beta < -\mathcal{O}(0.1)$ leads to the radius r_s and compactness $\mathcal{C} = \rho_c r_s^2/(6M_{\text{pl}}^2)$ larger than those in GR. The left panel of Fig. 1 corresponds to the 0-node solution with EOS $P/\rho_c = 2.78 \times 10^{-2}$ at $r = 0$. On using the GR solution (3.2), this translates to the compactness $\mathcal{C} = 0.05$. Solving the full background equations of motion, however, the actual value of compactness is found to be $\mathcal{C} = 0.29$. For the 0-node solution in Fig. 1, the pressure stays nearly constant up to the distance $r \simeq 0.06r_0$ due to the smallness of $f'(r)$ induced by the coupling β . This is followed by the decrease of $P(r)$ up to the surface $r_s = 0.1r_0$. This value is much larger than the corresponding radius $r_s = 0.04r_0$ in GR. Thus the nonvanishing 0-node solution can be distinguished from the GR solution in terms of r_s and \mathcal{C} .

The 1-node solution shown in the right panel of Fig. 1 leads to similar increases of r_s and \mathcal{C} relative to those in GR. In this case the term $-8\beta^2 A_c^2$ overwhelms $f_0 M_{\text{pl}}^2$ up to the distance $r = 0.05r_0$, so the function f decreases from $r = 0$ up to this distance. This results in the growth of $P(r)$ for $0 < r < 0.05r_0$. After the term $-8\beta^2 A_c^2$ becomes subdominant to $f_0 M_{\text{pl}}^2$ with the decrease of A_0 , the pressure starts to decrease toward the surface ($r_s = 0.09r_0$). As we will see in Sec. V for more realistic EOSs, there are cases in which f'/f remains positive for the 1-node solution. In such cases the pressure $P(r)$ decreases outwards, but the decreasing rate is smaller than that in GR and hence the radius r_s is larger.

The above discussion shows the importance of vector-field coupling on the metric component f , which in turns affects the radial dependence of pressure inside the star. Depending on the coupling β and central density ρ_c , the values of A_c allowing for the asymptotic behavior $A_0(r \rightarrow \infty) = 0$ are different. For decreasing A_c , both r_s and \mathcal{C} tend to approach those in GR.

IV. 0-NODE NS SOLUTIONS

We study the existence and property of 0-node solutions for realistic EOSs of NSs: SLy and BSk20. In Eq. (2.27), we introduced the dimensionless quantities y and z associated with ρ and P , respectively. The derivative of y with respect to $s = \ln(r/r_0)$, which is denoted as $y_{,s} = dy/ds$, is given by

$$y_{,s} = \frac{y}{z} \left(\frac{d\zeta}{d\xi} \right)^{-1} z_{,s} = -\frac{y(y+z)}{2z} \left(\frac{d\zeta}{d\xi} \right)^{-1} \frac{f_{,s}}{f}, \quad (4.1)$$

where we used Eq. (2.5) in the second equality. The dimensionless quantities f , $m = 3\mathcal{M}/(4\pi\rho_0 r_0^3)$, $\bar{A}_0 = A_0/M_{\text{pl}}$ obey the differential equations,

$$\frac{f_{,s}}{f} = \frac{2f(1-h) + 16\pi f e^{2s} z + 2\beta[\bar{A}_0^2 - h\bar{A}_0(\bar{A}_0 + 4\bar{A}_{0,s})] - h\bar{A}_{0,s}^2}{2h(f - \beta\bar{A}_0^2)}, \quad (4.2)$$

$$m_{,s} = \frac{3e^s(16\pi f e^{2s} y + h\bar{A}_{0,s}^2)}{16\pi(f - \beta\bar{A}_0^2)}, \quad (4.3)$$

$$\bar{A}_{0,ss} = \frac{\bar{A}_{0,s}[4\pi f(y+z)e^{2s} - fh + \beta\bar{A}_0^2 - \beta h\bar{A}_0\bar{A}_{0,s}] + 16\pi f \beta y e^{2s} \bar{A}_0}{h(f - \beta\bar{A}_0^2)}, \quad (4.4)$$

where

$$h = 1 - \frac{8\pi m}{3e^s}, \quad z = \exp\left[\frac{\zeta(\xi) - \alpha_3}{\alpha_2}\right], \quad (4.5)$$

with $\xi = \alpha_1 + \alpha_2 \ln y$. For EOSs (2.29), we solve the differential Eqs. (4.1)-(4.4) for y , f , m , and \bar{A}_0 under the boundary conditions (2.16)-(2.19) around $r = 0$. For a given negative coupling β and central density $y_c = \rho_c/\rho_0$, we search for the value of A_c at $r = 0$ approaching $A_0(r) \simeq 0$ for $r \gg r_s$. Numerically, the integration is performed up to the distance $r = 10^{12} r_0$.

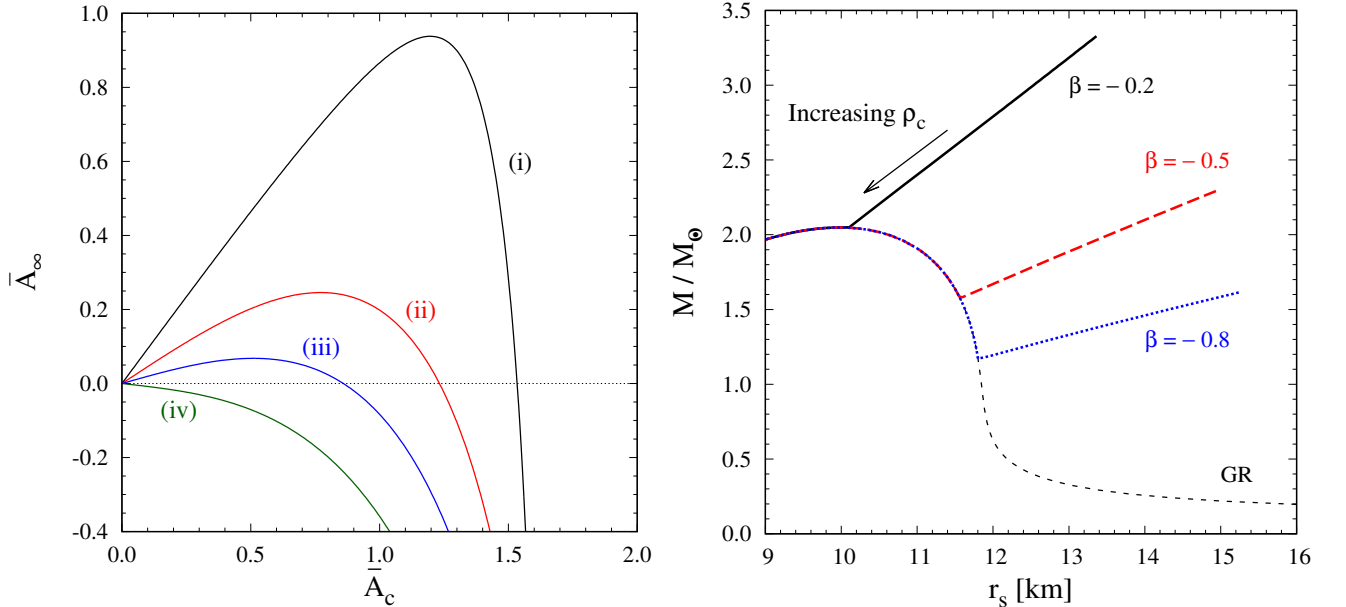


FIG. 2. (Left) The temporal vector component \bar{A}_∞ at $r \gg r_s$ versus its central value \bar{A}_c for SLy EOS with $\beta = -0.2$. Each plot corresponds to the central densities (i) $\rho_c = 2\rho_0$, (ii) $\rho_c = 8\rho_0$, (iii) $\rho_c = 12\rho_0$, and (iv) $\rho_c = 18\rho_0$, respectively. The dashed line represents $\bar{A}_\infty = 0$. (Right) The ADM mass M (in the unit of solar mass M_\odot) versus the radius r_s for SLy EOS with three different values of β . For $\beta = -0.2, -0.5, -0.8$, we consider the regimes of central densities $\rho_c \geq 8\rho_0$, $\rho_c \geq 4\rho_0$, and $\rho_c \geq 3\rho_0$, respectively. We also show how the values of M and r_s shift with the increase of ρ_c . The M - r_s relation in GR is represented as the thin black dashed line.

In the left panel of Fig. 2, we plot the asymptotic value $\bar{A}_\infty = A_\infty/M_{\text{pl}}$ at $r \gg r_s$ versus $\bar{A}_c = A_c/M_{\text{pl}}$ at $r = 0$ for SLy EOS with $\beta = -0.2$. The curve (i), which corresponds to the central density $\rho_c = 2\rho_0$, has two intersections with the line $\bar{A}_\infty = 0$, i.e., $\bar{A}_c = 0$ and $\bar{A}_c = 1.53$. The former is the GR branch, while the latter is the 0-node solution. In Fig. 2, we observe that the positive change of \bar{A}_c from the GR branch leads to the positive shift of \bar{A}_∞ . On the other hand, the positive change of \bar{A}_c from the 0-node solution results in the negative shift of \bar{A}_∞ . In Fig. 6 of Ref. [47], the similar behavior was found for polytrope EOS in different vector-tensor theories. In such cases the authors of Ref. [47] showed that the GR solution is stable by considering axial and polar parity perturbations, so it is unlikely that the 0-node solution arises as the consequence of tachyonic instabilities of the GR solution. Rather, the 0-node solution discovered in our GP theories may be induced by some nonlinear effects such as the selected choice of initial conditions.

The values of \bar{A}_c corresponding to the 0-node branch get smaller for larger ρ_c , see cases (ii) and (iii) in the left panel of Fig. 2. For $\beta = -0.2$, this nonvanishing A_0 solution disappears above the critical density $\bar{\rho}_c \simeq 16\rho_0$, in which regime only the GR branch is left. The case (iv) in Fig. 2 corresponds to such an example. For the coupling β of order -0.1 , we find that the 0-node solution is present for both SLy and BSk20 EOSs and that the $(\bar{A}_\infty, \bar{A}_c)$ relation is similar to that shown in Fig. 2. Below a critical central density $\bar{\rho}_c$ (which depends on the coupling β), there exist both GR and 0-node branches, with theoretical curves in the $(\bar{A}_\infty, \bar{A}_c)$ plane convex upward.

This property is very different from the 0-node solution in scalar-tensor theories. As we will briefly review in Appendix, scalarized solutions in scalar-tensor theories do not appear below a critical central density ρ_{c1} . For $\rho_c < \rho_{c1}$, the field value ϕ_∞ at $r \gg r_s$ monotonically increases with the growth of central value ϕ_c from the GR point $(\phi_\infty, \phi_c) = (0, 0)$. In this regime, the GR solution is stable. Above the critical density ρ_{c1} , the theoretical curves in the (ϕ_∞, ϕ_c) plane, which are convex downward, enter the region $\phi_\infty < 0$, so that the 0-node solution appears besides the GR branch. In the left panel of Fig. 5 in Appendix, this transition can be seen from the curve (i) to (ii), where the latter has two intersecting points at $\phi_\infty = 0$. In case (ii), the GR branch $\phi_c = 0$ can be unstable to undergo spontaneous scalarization to the 0-node solution with $\phi_c \neq 0$. Above a second critical density ρ_{c2} , the theoretical curves in the (ϕ_∞, ϕ_c) plane again enter the region $\phi_\infty > 0$ and hence there is only the GR solution in this regime (see case (v) in Fig. 5). The 0-node solution in scalar-tensor theories, which can arise out of spontaneous scalarization from the GR branch, exists for $\rho_{c1} < \rho_c < \rho_{c2}$. In the numerical simulation of Fig. 5 in Appendix, $\rho_{c1} = 4.3\rho_0$ and $\rho_{c2} = 14.4\rho_0$.

In GP theories, the fact that the convex-upward curves in the $(\bar{A}_\infty, \bar{A}_c)$ plane have the intersection point $\bar{A}_c > 0$ with $\bar{A}_\infty = 0$ is related to the property that $A_0(r)$ always decreases as a function of r around $r = 0$, see Eq. (2.19). Moreover, the term $-8\beta^2 A_c^2$ in Eq. (2.16) always works to slow down the decrease of $P(r)$. This is attributed to the slower increase of f'/f as compared to the GR branch. These properties are different in scalar-tensor theories, in that the behavior of $\phi(r)$ and $P(r)$ depends on whether EOS is in the range $\rho_c > 3P_c$ or not (see Appendix). For $\rho_c < 3P_c$, the scalar field $\phi(r)$ increases as a function of r deep inside the star, but this is not the case for $A_0(r)$ in GP theories. As we see in the left panel of Fig. 2, the nonvanishing vector-field configuration with A_c of order M_{pl} is present for a wide range of ρ_c below the critical value $\bar{\rho}_c \simeq 16\rho_0$.

In the right panel of Fig. 2, we show the mass M versus the radius r_s for three different values of β . When $\beta = -0.2$, the range of ρ_c plotted in the figure is $\rho_c \geq 8\rho_0$. In this range of ρ_c the derivative f'/f is positive inside the star, so that the pressure $P(r)$ decreases outwards. Even for $\rho_c = 8\rho_0$, we have $M = 3.33M_\odot$ and $r_s = 13.4$ km, both of which are larger than the corresponding values $M = 1.74M_\odot$ and $r_s = 11.4$ km in GR. These changes are mostly attributed to the fact that the slow decrease of $P(r)$ induced by the coupling β leads to larger r_s . If we consider ρ_c lower than $8\rho_0$, the quantity f'/f around $r = 0$ further gets smaller and hence both M and r_s are greater than those for $\rho_c = 8\rho_0$. As ρ_c increases in the region $\rho_c \geq 8\rho_0$, M and r_s decrease and they finally approach those in GR. This is consistent with the fact that the value of A_c for the 0-node solution decreases for increasing ρ_c in the left panel of Fig. 2 and only the GR branch is left for $\rho_c > 16\rho_0$.

As the coupling $|\beta|$ increases, the range of ρ_c allowing for the nonvanishing VS is limited to the region with low densities. For $\beta = -0.5$ and $\beta = -0.8$, the 0-node solution with M and r_s different from those in GR exists for $\rho_c \lesssim 7\rho_0$ and $\rho_c \lesssim 5\rho_0$, respectively. In Fig. 2 we can confirm that, for larger $|\beta|$ (of order 0.1), the deviation from the GR values of M and r_s in high-density regions tends to be smaller. This behavior is also consistent with the results found in Ref. [47] in different vector-tensor theories. For $|\beta| = \mathcal{O}(1)$ the 0-node solution tends to disappear, but the 1-node solution starts to appear as we already discussed in Sec. III. The numerical results shown in Fig. 2 are obtained for SLy EOS, but we confirmed that the similar property also holds for BSk20 EOS and hence the results are insensitive to the choice of EOSs.

In order to check whether the 0-node solution discussed above is gravitationally bound, we compute the proper mass,

$$M_p = \int_0^{r_s} \frac{4\pi\rho r^2}{\sqrt{h}} dr. \quad (4.6)$$

The gravitational binding energy is given by $\Delta = M_p - M$. For the 0-node branch corresponding to the numerical simulation of Fig. 2, we find that Δ is generally positive. Then, the necessary condition for gravitational stability is at least satisfied. However, we need to consider the axial and polar perturbations to judge the stability of solutions properly. In addition, it is not yet clear whether the 0-node solutions constructed above can be realized from certain initial data or not. It is beyond the scope of our paper to address these issues.

V. 1-NODE NS SOLUTIONS

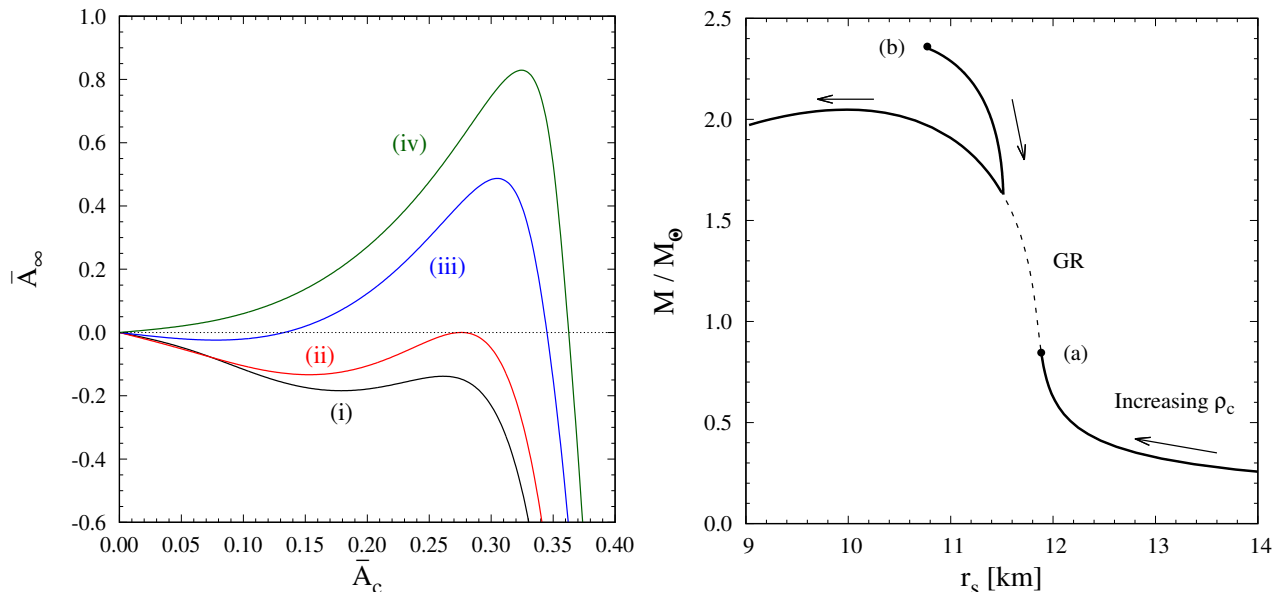


FIG. 3. (Left) \bar{A}_∞ versus \bar{A}_c for SLy EOS with $\beta = -5$. Each plot corresponds to the central densities (i) $\rho_c = 3\rho_0$, (ii) $\rho_c = 3.74\rho_0$, (iii) $\rho_c = 6\rho_0$, and (iv) $\rho_c = 8\rho_0$, respectively. The dashed line represents $\bar{A}_\infty = 0$. (Right) M/M_\odot versus the radius r_s for SLy EOS with $\beta = -5$. When ρ_c exceeds the critical value $\hat{\rho}_{c1} = 3.74\rho_0$, the 1-node VS appears as the intersection point of theoretical curves in the $(\bar{A}_\infty, \bar{A}_c)$ plane with $\bar{A}_\infty = 0$, i.e., case (ii) in the left panel. At $\rho_c = \hat{\rho}_{c1}$, the GR point (a) jumps to the other point (b) in the (M, r_s) plane. As ρ_c increases further, the nonzero \bar{A}_c corresponding to the smaller intersection value with $\bar{A}_\infty = 0$ tends to decrease toward $\bar{A}_c = 0$. Above the critical density $\hat{\rho}_{c2} = 7.1\rho_0$, M and r_s are identical to those in GR.

We then proceed to the investigation of 1-node solutions for SLy and BSk20 EOSs. As a function of r , the temporal vector component of 1-node solutions crosses $A_0(r) = 0$ once at a finite radius and approaches $A_0(r) \rightarrow 0$ at spatial infinity. As in the case of constant density ρ discussed in Sec. III, our numerical computation shows that the 1-node solution exists for $\beta = -\mathcal{O}(1)$.

In the left panel of Fig. 3, we plot the asymptotic value $\bar{A}_\infty = A_\infty/M_{\text{pl}}$ for $r \gg r_s$ versus $\bar{A}_c = A_c/M_{\text{pl}}$ at $r = 0$ for SLy EOS with $\beta = -5$ by choosing several different central densities ρ_c . In case (i), which corresponds to $\rho_c = 3\rho_0$, there is only the GR branch characterized by $\bar{A}_\infty = 0$ and $\bar{A}_c = 0$. As ρ_c increases, the intersection with the line $\bar{A}_\infty = 0$ starts to appear at $\bar{A}_c > 0$ for ρ_c exceeding the critical density $\hat{\rho}_{c1} = 3.74\rho_0$. The nonvanishing VS for $\rho_c = \hat{\rho}_{c1}$ has the value $\bar{A}_c = 0.2741$, see case (ii) in Fig. 3. In the right panel of Fig. 3, we plot M versus r_s for $\beta = -5$ with SLy EOS. We observe that there is a jump from the GR point (a) to the VS (b) at $\rho_c = \hat{\rho}_{c1}$. This is attributed to the fact that the nonvanishing VS suddenly appears as in case (ii) on the left panel of Fig. 3.

From point (a) to (b), the radius r_s is slightly decreased from 11.9 km to 10.8 km, but the mass M is increased from $0.85M_\odot$ to $2.36M_\odot$. This behavior mostly arises from the nontrivial radial dependence of ρ . On the VS (b), the coupling $|\beta|$ of order 1 leads to the increase of $P(r)$ as a function of r around $r = 0$, which is associated with the decrease of $f(r)$, see Eqs. (2.16) and (2.18). This is also accompanied by the growth of $\rho(r)$ with r deep inside NS. While $\rho(r)$ starts to decrease around the surface of NSs, the quantity $y = \rho/\rho_0$, which appears in Eq. (4.3), is larger than that in GR in most internal regions of the star. This results in the mass M for the VS (b) greater than that of the GR point (a). For the VS (b), the decrease of $P(r)$ around the surface of star occurs more rapidly in comparison to GR, so the radius r_s is even smaller than that of point (a).

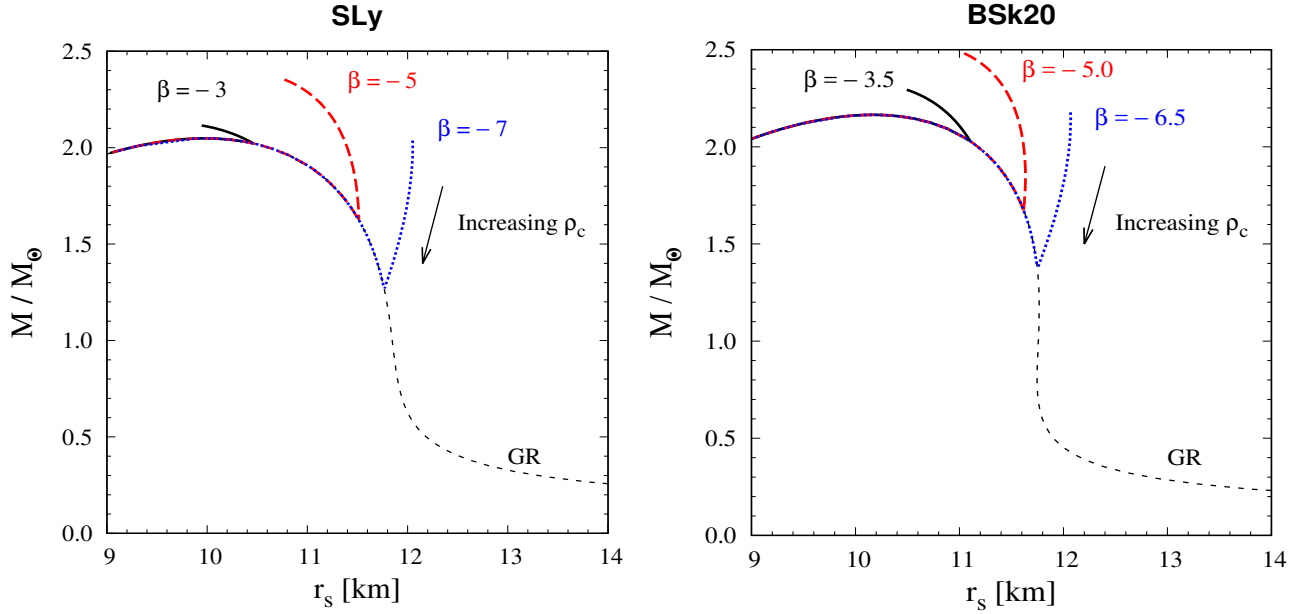


FIG. 4. (Left) M/M_\odot versus the radius r_s for SLy EOS with several different values of β . For $\beta = -3, -5, -7$, the ranges of ρ_c plotted in the figure are $\rho_c > 12.32\rho_0$, $\rho_c > 3.74\rho_0$, and $\rho_c > 1.5\rho_0$, respectively. (Right) M/M_\odot versus the radius r_s for BSk20 EOS. For $\beta = -3.5, -5.0, -6.5$, we consider the density regions $\rho_c > 8.15\rho_0$, $\rho_c > 3.41\rho_0$, and $\rho_c > 1.66\rho_0$, respectively.

For ρ_c exceeding $\hat{\rho}_{c1} = 3.74\rho_0$, we observe in case (iii) of Fig. 3 that the two intersection points with $\bar{A}_\infty = 0$ start to appear besides the GR branch. The root with smaller \bar{A}_c (denoted as P_s) has a similar property to the scalarized solution in scalar-tensor theories (see Appendix), in that the positive shift of \bar{A}_c gives the positive change of \bar{A}_∞ . On the other hand, the root with larger \bar{A}_c (denoted as P_l) has an opposite characteristic, similar to the 0-node solution studied in Sec. IV. We also note that, under the shift $\bar{A}_c > 0$, the GR point in case (iii) moves to the direction $\bar{A}_\infty < 0$. With these properties, there is a possibility that the GR branch can be unstable to reach the point P_s . On the other hand, the solution P_l should arise from some nonlinear effects rather than spontaneous vectorization.

Since the value \bar{A}_c for the root P_s gets smaller for increasing ρ_c , the effect of coupling β on modifying the structure of NSs tends to be weaker. In the right panel of Fig. 3, we plot the values of M and r_s corresponding to the root P_s . As ρ_c increases from point (b), both M and r_s approach those in GR. Above the critical density $\hat{\rho}_{c2} = 7.1\rho_0$, the root P_s disappears, see case (iv) in Fig. 3. For $\rho_c > \hat{\rho}_{c2}$, the theoretical curve in the (M, r_s) plane is identical to that in GR. The difference from the GR solution is present for the density in the range $\hat{\rho}_{c1} < \rho_c < \hat{\rho}_{c2}$. For ρ_c close to $\hat{\rho}_{c2}$, the pressure $P(r)$ decreases as a function of r along with the increase of $f(r)$.

In the left panel of Fig. 4, we plot the mass-radius relation for SLy EOS with $\beta = -3, -5, -7$. When $\beta = -3$, the root P_s explained above exists for the central density $12.32\rho_0 < \rho_c < 13.4\rho_0$. In this region, the values of M and r_s are different from those in GR, but their modifications are not so significant compared to the coupling $\beta = -5$. As $|\beta|$ increases, the 1-node solution is present for smaller central densities, e.g., $3.74\rho_0 < \rho_c < 7.1\rho_0$ for $\beta = -5$. When $\beta = -7$, the existence of the 1-node branch is numerically confirmed even for small ρ_c close to ρ_0 . In Fig. 4, the plotted values of M and r_s for $\beta = -7$ correspond to the density region $\rho_c > 1.5\rho_0$. In this case, the 1-node solution disappears above the critical density $\hat{\rho}_{c2} = 5.3\rho_0$. Thus, for increasing $|\beta|$, the M - r_s relation at higher densities is hardly modified in comparison to GR. For $|\beta|$ exceeding the order of 10, the 1-node solution tends to disappear, but the 2-node solution starts to appear.

The right panel of Fig. 4 shows the theoretical values of M and r_s for BSk20 EOS with $\beta = -3.5, -5.0, -6.5$. For larger $|\beta|$, the modification from GR occurs at smaller central densities in a similar way to SLy EOS with $\beta = -\mathcal{O}(1)$. Thus, the properties of 1-node solutions as well as 0-node solutions are insensitive to the choice of NS EOSs. We also compute the gravitational binding energy $\Delta = M_p - M$ for 1-node solutions and find that the necessary condition $\Delta > 0$ for gravitational stability is satisfied for the cases plotted in Fig. 4.

Before closing this section, we would like to discuss whether the 1-node solutions can be the endpoints of tachyonic instability of the GR solutions with $A_\mu = 0$. As we have already seen in Sec. III, the value of β for the existence of 1-node solutions is somewhat consistent with the value for the onset of tachyonic instability of the GR solution. The possibility that the fundamental solution is given by 1-node solutions may not be surprising. For instance, in

spherically symmetric Proca stars the temporal component of the vector field has a single node [75], while in the scalar boson stars the scalar field has 0 nodes [76]. However, this would not ensure that 1-node solutions are the endpoints of tachyonic instability of the GR star solutions in our model.

We have observed several qualitative differences between 1-node solutions and scalarized solutions in the M - r_s relation (see Appendix). First, in the region of low densities, the 1-node branch in GP theories is disconnected to the GR branch in the M - r_s diagram, while the scalarized branch is smoothly connected to the latter. Spontaneous scalarization occurs via a continuous bifurcation from the GR solution and may be regarded as a continuous phase transition with the order parameter ϕ , in analogy with spontaneous magnetization in ferromagnetic materials. On the other hand, it seems more plausible that, even if the 1-node solution is realized as the consequence of an instability of the GR solution, it may be formed via a mechanism like a first-order phase transition, rather than a continuous transition. Another possibility is that 1-node solutions may be formed from a selected choice of initial conditions as in the case of 0-node solutions. There is also an alternative possibility that vectorized solutions possess nonzero radial and angular components of the vector field satisfying the asymptotic condition $A_\mu(r \rightarrow \infty) = 0$. In Hellings and Nordtvedt theory, Ref. [47] showed that the tachyonic instability of GR solutions arises for the modes with multipole indices $\ell \geq 1$. The construction of such solutions is beyond the scope of our paper.

VI. CONCLUSIONS

In this paper, we investigated NS solutions in GP theories given by the action (2.1) with the vanishing longitudinal vector component ($A_1 = 0$). The deviation from GR arises from the nonvanishing temporal vector component A_0 in the vicinity of NSs, with the asymptotic behavior $A_0 \rightarrow 0$ at spatial infinity. The model (2.14) allows for the existence of NS solutions with a nontrivial profile of the vector field (2.13) besides the GR solutions with $A_0 = 0$ everywhere. In addition to relativistic stars with constant density ρ , we considered SLy and BSk20 EOSs to describe the realistic nuclear interaction inside NSs.

In Sec. III, we first studied the vector-field solution for relativistic stars with constant ρ to understand its general properties semi-analytically. Inside the star, the temporal vector component obeys Eq. (3.4), which possesses the GR branch. The necessary condition for the realization of spontaneous vectorization to a nonvanishing A_0 solution corresponds to $\beta < 0$. Under the conditions (3.6) and (3.7), Eq. (3.4) reduces to Eq. (3.8), whose solutions inside and outside the star are given by Eqs. (3.9) and (3.12) respectively. However, the approximations (3.6) and (3.7) lose their validities for compactness of the star \mathcal{C} of order 0.1. In particular, the deviation of metric components f and h from 1 leads to the decrease of $A_0(r)$ inside the star faster than that estimated by Eqs. (3.9). This results in the existence of nonvanishing vector-field solutions even for the coupling $|\beta|$ smaller than the order 1.

For $\beta = -\mathcal{O}(0.1)$, we numerically confirmed the existence of 0-node solutions where A_0 monotonically decreases toward the asymptotic value 0 at spatial infinity. In Fig. 1, we observe that the 0-node has a positive scalar charge Q . For $\beta = -\mathcal{O}(1)$, there exists the 1-node solution where A_0 crosses 0 once and then approaches 0 as $r \rightarrow \infty$. The 1-node possesses a negative scalar charge. The n -nodes with $n \geq 2$ only arise for the large coupling in the range $\beta < -\mathcal{O}(10)$. Although we considered the constant-density star in Sec. III, these properties are independent of the choice of EOSs.

In Sec. IV, we discussed the property of 0-node solutions and the mass-radius relation by considering SLy and BSk20 EOSs for $\beta = -\mathcal{O}(0.1)$. As we see in the left panel of Fig. 2, below a critical central density $\bar{\rho}_c$, there exists the 0-node solution with $\bar{A}_c > 0$ and $\bar{A}_\infty = 0$ besides the GR branch. However, the convex-upward property of theoretical curves in the $(\bar{A}_\infty, \bar{A}_c)$ plane for the 0-node is different from that of scalar-tensor theories in the $(\bar{\phi}_\infty, \bar{\phi}_c)$ plane (see the left panel of Fig. 5). Analogous to the discussion of Ref. [47], we argue that the GR branch should be stable and hence the 0-node solution may arise from some nonlinear effects rather than from spontaneous vectorization. The coupling β works to slow down the decrease of pressure inside the star, so the radius r_s and mass M corresponding to the 0-node solution are greater than those of the GR branch. For increasing $|\beta|$ of order 0.1, the deviation from the GR values of M and r_s occurs in the region of lower densities.

In Sec. V, we showed the existence of 1-node solutions for $\beta = -\mathcal{O}(1)$ with SLy and BSk20 EOSs. The 1-node suddenly arises above a critical density $\hat{\rho}_{c1}$ and disappears above a second critical density $\hat{\rho}_{c2}$. For the density in the range $\hat{\rho}_{c1} < \rho_c < \hat{\rho}_{c2}$, there are two roots of $\bar{A}_\infty = 0$, P_s and P_l in the $(\bar{A}_\infty, \bar{A}_c)$ plane, besides the GR branch. The root P_s has a property similar to the scalarized solution in scalar-tensor theories, so there is a possibility that the former arises out of spontaneous vectorization. The mass M corresponding to root P_s is larger than that in GR and, as ρ_c increases toward $\hat{\rho}_{c2}$, M approaches the GR value. For larger $|\beta|$, the deviation of M and r_s from those in GR is limited to lower-density regions.

Here, we would like to emphasize that the existence and qualitative properties of the 0-node and 1-node solutions are insensitive to different choices of EOSs. As we see in Eq. (2.19), the temporal vector component $A_0(r)$ around the center of NS is mostly determined by the values of ρ_c and β . Since the central pressure P_c does not appear for

this solution up to the order $\mathcal{O}(r^4)$, the different choice of EOSs hardly affects the behavior of the vector-field profile around the center of NS. On the other hand, the iterative solution (2.16) of $P(r)$ is affected by the value of P_c as well as ρ_c and β . Thus, the radius and mass of NS can be modified by choosing different EOSs, but the qualitative behavior of vectorized solutions are insensitive to the change of EOSs. It is of interest to study observational signatures of these solutions through the gravitational wave measurements. For vectorized solutions the mass-radius relation differs from that in GR, so the tidal Love number of NSs [78–81] is also subject to modifications. This can be potentially tested in the GW observations of NS mergers.

It is not clear yet whether 1-node solutions constructed in this paper are indeed the endpoints of tachyonic instability of the GR star, namely, vectorized NS solutions. Further studies will be needed to clarify this issue. First, it will be very crucial to investigate whether the 0-node and 1-node solutions found in this paper are stable against axial and polar perturbations. Second, it will also be important to construct NS solutions with the nonvanishing radial and angular components of the vector field satisfying $A_\mu(r \rightarrow \infty) = 0$ and, if they exist, check their stability.

On the other hand, the 0-node and 1-node solutions constructed in this paper deserve for further studies from various aspects, e.g., the extension to rotating solutions and the analysis regarding the tidal deformability and universal relations [83–87] (see also [88] and references therein). They would be helpful to distinguish the solutions in GP theories from GR and other modified theories of gravitation from the theoretical and observational viewpoints. Another possible issue is that, assuming the vector field triggering spontaneous vectorization exists since the beginning of the Universe, the same coupling can potentially induce tachyonic growth of the vector field over the cosmic expansion history, which might result in the conflict with Solar System tests of gravity. The similar issue has already been pointed out in the case of spontaneous scalarization [89–92]. In vector-tensor theories, the problem may be more serious as the vector field has more degrees of freedom and it can also break the isotropy of the Universe. We hope to come back to these issues in our future work.

ACKNOWLEDGEMENTS

RK is supported by the Grant-in-Aid for Young Scientists B of the JSPS No.17K14297. ST is supported by the Grant-in-Aid for Scientific Research Fund of the JSPS No.19K03854 and MEXT KAKENHI Grant-in-Aid for Scientific Research on Innovative Areas ‘‘Cosmic Acceleration’’ (No.15H05890). MM was supported by the research grant under the Decree-Law 57/2016 of August 29 (Portugal) through the Fundação para a Ciência e a Tecnologia. MM is also grateful for the hospitality at the Tokyo University of Science where this work was initiated.

APPENDIX: SPONTANEOUS SCALARIZATION IN SCALAR-TENSOR THEORIES

In comparison to the VS in GP theories, we briefly review spontaneous scalarization in scalar-tensor theories. Let us consider the action in the Jordan frame (given by the metric $g_{\mu\nu}$),

$$\mathcal{S} = \int d^4x \sqrt{-g} \left[\frac{M_{\text{pl}}^2}{2} F(\phi) R - \frac{1}{2} \omega(\phi) g^{\mu\nu} \partial_\mu \phi \partial_\nu \phi \right] + \mathcal{S}_m(g_{\mu\nu}, \Psi_m), \quad (\text{A.1})$$

where $F(\phi)$ and $\omega(\phi)$ are functions of the scalar field ϕ . In this frame, the matter fields are minimally coupled to gravity. Under the conformal transformation $(g_{\mu\nu})_E = F(\phi) g_{\mu\nu}$, the action (A.1) is transformed to

$$\mathcal{S} = \int d^4x \sqrt{-g_E} \left[\frac{M_{\text{pl}}^2}{2} R_E - \frac{1}{2} (g^{\mu\nu})_E \partial_\mu \varphi \partial_\nu \varphi \right] + \mathcal{S}_m(F^{-1}(\phi)(g_{\mu\nu})_E, \Psi_m), \quad (\text{A.2})$$

where the subscript ‘‘E’’ represents quantities in the Einstein frame, and

$$\frac{d\varphi}{d\phi} = \sqrt{\frac{3}{2} \left(\frac{M_{\text{pl}} F_{,\phi}}{F} \right)^2 + \frac{\omega}{F}}. \quad (\text{A.3})$$

We choose the canonical scalar field φ in the Einstein frame such that $\varphi = \phi$. Since $\omega = [1 - 3M_{\text{pl}}^2 F_{,\phi}^2 / (2F^2)] F$ in this case, the Jordan-frame action (A.1) is expressed as

$$\mathcal{S} = \int d^4x \sqrt{-g} \left[\frac{M_{\text{pl}}^2}{2} F(\phi) R - \frac{1}{2} \left(1 - \frac{3M_{\text{pl}}^2 F_{,\phi}^2}{2F^2} \right) F(\phi) g^{\mu\nu} \partial_\mu \phi \partial_\nu \phi \right] + \mathcal{S}_m(g_{\mu\nu}, \Psi_m). \quad (\text{A.4})$$

The nonminimal coupling chosen by Damour and Esposito-Farese [24, 25] corresponds to

$$F(\phi) = e^{-\beta\phi^2/(2M_{\text{pl}}^2)}, \quad (\text{A.5})$$

where β is a constant.

In full Horndeski theories including the action (A.4) as a special case, the full background equations of motion on the spherically symmetric and static background (2.2) were already derived in the literature, see, e.g., Eqs. (8)-(10) of Ref. [77]. We do not write them explicitly here. The pressure P and density ρ obey the same continuity equation as (2.5). The relation between P and ρ can be specified by a given EOS. For the nonminimal coupling (A.5), there exists the scalarized solution with $\phi(r) \neq 0$ besides the GR branch $\phi(r) = 0$. On using the expansion similar to Eq. (2.15) around $r = 0$, the iterative scalarized solutions to P , h , f , and ϕ deep inside the star are given by

$$P(r) = P_c - \frac{(\rho_c + P_c)[2M_{\text{pl}}^2(\rho_c + 3P_c) + \beta^2\phi_c^2(\rho_c - 3P_c)]}{24M_{\text{pl}}^4} e^{\beta\phi_c^2/(2M_{\text{pl}}^2)r^2} + \mathcal{O}(r^4), \quad (\text{A.6})$$

$$h(r) = 1 - \frac{2M_{\text{pl}}^2\rho_c - \beta^2\phi_c^2(\rho_c - 3P_c)}{6M_{\text{pl}}^4} e^{\beta\phi_c^2/(2M_{\text{pl}}^2)r^2} + \mathcal{O}(r^4), \quad (\text{A.7})$$

$$f(r) = f_0 + \frac{f_0[2M_{\text{pl}}^2(\rho_c + 3P_c) + \beta^2\phi_c^2(\rho_c - 3P_c)]}{12M_{\text{pl}}^4} e^{\beta\phi_c^2/(2M_{\text{pl}}^2)r^2} + \mathcal{O}(r^4), \quad (\text{A.8})$$

$$\phi(r) = \phi_c + \frac{\beta\phi_c(\rho_c - 3P_c)}{12M_{\text{pl}}^2} e^{\beta\phi_c^2/(2M_{\text{pl}}^2)r^2} + \mathcal{O}(r^4), \quad (\text{A.9})$$

where ϕ_c is the field value at $r = 0$. At spatial infinity, the scalar field behaves as $\phi(r) \simeq \phi_\infty + Q/r$, where ϕ_∞ and Q are constants. The internal and external solutions to $\phi(r)$ are joined each other at the stellar radius r_s . It is known that the 0-node scalarized solution with $\phi_\infty \simeq +0$ is present for negative β in the range $\beta < -4.35$ [26–28].

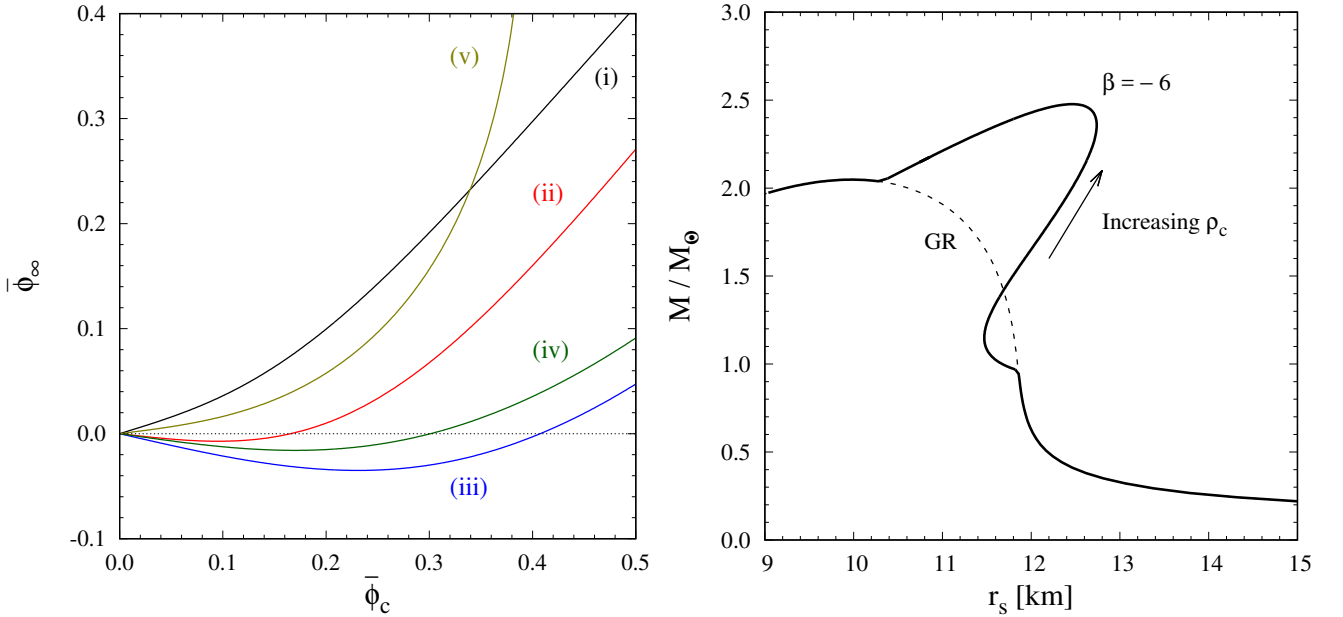


FIG. 5. (Left) The scalar field $\bar{\phi}_\infty = \phi_\infty/M_{\text{pl}}$ at spatial infinity versus the central value $\bar{\phi}_c = \phi_c/M_{\text{pl}}$ at $r = 0$ for SLy EOS with $\beta = -6$. Each line corresponds to the central densities (i) $\rho_c = 3\rho_0$, (ii) $\rho_c = 5\rho_0$, (iii) $\rho_c = 10\rho_0$, (iv) $\rho_c = 12\rho_0$, and (v) $\rho_c = 16\rho_0$, respectively. The dashed line represents $\bar{\phi}_\infty = 0$. (Right) M/M_\odot versus r_s for SLy EOS with $\beta = -6$. We also show how the values of M and r_s move with the increase of ρ_c . The mass-radius relation in GR is represented as the thin black dashed line.

Let us consider SLy EOS with the coupling $\beta = -6$. In the left panel of Fig. 5, we plot $\bar{\phi}_\infty = \phi_\infty/M_{\text{pl}}$ versus $\bar{\phi}_c = \phi_c/M_{\text{pl}}$ for five different central densities ρ_c . The line (i), which corresponds to $\rho_c = 3\rho_0$, has the intersection with $\bar{\phi}_\infty = 0$ only at the GR point $\bar{\phi}_c = 0$. For $\rho_c \gtrsim 4.3\rho_0$, the scalarized solution with $\bar{\phi}_c > 0$ and $\bar{\phi}_\infty = 0$ starts to appear besides the GR branch. Unlike the 0-node solution in GP theories, the line (ii) in Fig. 5 is convex downward. In this case, the GR solution can be unstable to undergo spontaneous scalarization to the other branch with $\bar{\phi}_c \neq 0$.

In the right panel of Fig. 5, we plot the mass M and radius r_s of NS for $\beta = -6$, which agrees with the result presented in Fig. 1 of Ref. [82]. The mass-radius relation is similar to that in GR for the central density in the range $\rho_c \lesssim 4.3\rho_0$, but the difference starts to appear for $\rho_c > 4.3\rho_0$ due to the emergence of the scalarized branch. The radius r_s associated with the scalarized solution in the range $4.3\rho_0 < \rho_c \lesssim 7\rho_0$ is smaller than the corresponding value of the GR branch. This is attributed to the fact that $3P_c$ is smaller than ρ_c in this regime and hence the term $\beta^2\phi_c^2(\rho_c - 3P_c)$ in Eq. (A.6) leads to the decreasing rate of $P(r)$ larger than that in GR. As ρ_c increases further, the term $3P_c$ cannot be negligible relative to ρ_c . In particular, for $\rho_c \gtrsim 10\rho_0$, EOS enters the fully relativistic region with $\rho_c < 3P_c$. Then, the term $\beta^2\phi_c^2(\rho_c - 3P_c)$ is negative with $e^{\beta\phi_c^2/(2M_{\text{pl}}^2)} < 1$ for $\phi_c \neq 0$, so the decreasing rate of $P(r)$ becomes smaller than that in GR deep inside the star. This results in the larger radius r_s for the scalarized solution relative to that of the GR branch. Indeed, the increase of r_s and M seen in Fig. 5 (in comparison to their GR values) mostly arises from this slower decrease of $P(r)$.

In the left panel of Fig. 5, we observe that the field ϕ_c of the scalarized solution reaches the maximum value $0.4M_{\text{pl}}$ around $\rho_c \simeq 10\rho_0$. Since $\rho_c - 3P_c < 0$ for $\rho_c \gtrsim 10\rho_0$, the iterative solution (A.9) shows that $\phi(r)$ increases as a function of r deep inside NSs. Around the surface of star the term $3P$ becomes smaller than ρ , so that $\phi(r)$ decreases to join the exterior solution at $r = r_s$. For increasing ρ_c , however, this growth of $\phi(r)$ tends to occur up to $r = r_s$ and hence it becomes more difficult to smoothly connect to the external solution. Reflecting this point, the field value ϕ_c of scalarized solutions decreases for increasing ρ_c in the range $\rho_c \gtrsim 10\rho_0$, see case (iv) of Fig. 5. Eventually, the scalarized solution with $\phi_c > 0$ disappears for $\rho_c > 14.4\rho_0$. The case (v) in Fig. 5 corresponds to such an example, which possesses only the GR branch. In the right panel of Fig. 5, the mass-radius relation approaches that of GR in this high-density region. The above discussion shows that the scalarized solution is present in the range $4.3\rho_0 < \rho_c < 14.4\rho_0$ for SLy EOS with $\beta = -6$. The property of scalarized solutions discussed above also holds for other EOSs entering the full relativistic regime $\rho_c < 3P_c$ as ρ_c increases.

-
- [1] B. P. Abbott *et al.* [LIGO Scientific and Virgo Collaborations], Phys. Rev. Lett. **116**, 061102 (2016) [arXiv:1602.03837 [gr-qc]].
- [2] C. Lange *et al.*, Mon. Not. Roy. Astron. Soc. **326**, 274 (2001) [astro-ph/0102309].
- [3] B. P. Abbott *et al.* [LIGO Scientific and Virgo Collaborations], Phys. Rev. Lett. **119**, 161101 (2017) [arXiv:1710.05832 [gr-qc]].
- [4] T. E. Riley *et al.*, Astrophys. J. Lett. **887**, L21 (2019) [arXiv:1912.05702 [astro-ph.HE]].
- [5] G. Raaijmakers *et al.*, Astrophys. J. Lett. **887**, L22 (2019) [arXiv:1912.05703 [astro-ph.HE]].
- [6] T. Baker, E. Bellini, P. Ferreira, M. Lagos, J. Noller and I. Sawicki, Phys. Rev. Lett. **119** (2017) no.25, 251301 [arXiv:1710.06394 [astro-ph.CO]].
- [7] A. A. Starobinsky, Phys. Lett. B **91**, 99 (1980).
- [8] P. G. Bergmann, Int. J. Theor. Phys. **1**, 25 (1968).
- [9] T. V. Ruzmaikina and A. A. Ruzmaikin, Zh. Eksp. Teor. Fiz., **57**, 680, (1969).
- [10] A. De Felice and S. Tsujikawa, Living Rev. Rel. **13**, 3 (2010) [arXiv:1002.4928 [gr-qc]].
- [11] A. Cooney, S. DeDeo and D. Psaltis, Phys. Rev. D **82**, 064033 (2010) [arXiv:0910.5480 [astro-ph.HE]].
- [12] A. S. Arapoglu, C. Deliduman and K. Y. Eksi, JCAP **1107**, 020 (2011) [arXiv:1003.3179 [gr-qc]].
- [13] M. Orellana, F. Garcia, F. A. Teppa Pannia and G. E. Romero, Gen. Rel. Grav. **45**, 771 (2013) [arXiv:1301.5189 [astro-ph.CO]].
- [14] A. V. Astashenok, S. Capozziello and S. D. Odintsov, JCAP **1312**, 040 (2013) [arXiv:1309.1978 [gr-qc]].
- [15] S. S. Yazadjiev, D. D. Doneva, K. D. Kokkotas and K. V. Staykov, JCAP **1406**, 003 (2014) [arXiv:1402.4469 [gr-qc]].
- [16] M. Aparicio Resco, A. de la Cruz-Dombriz, F. J. Llanes Estrada and V. Zapatero Castrillo, Phys. Dark Univ. **13**, 147 (2016) [arXiv:1602.03880 [gr-qc]].
- [17] R. Kase and S. Tsujikawa, JCAP **1909**, 054 (2019) [arXiv:1906.08954 [gr-qc]].
- [18] A. Ganguly, R. Gannouji, R. Goswami and S. Ray, Phys. Rev. D **89**, 064019 (2014) [arXiv:1309.3279 [gr-qc]].
- [19] C. Brans and R. H. Dicke, Phys. Rev. **124**, 925 (1961).
- [20] Y. Fujii and K. Maeda, “The scalar-tensor theory of gravitation”, Cambridge University Press (2003).
- [21] T. Kobayashi and T. Hiramatsu, Phys. Rev. D **97** (2018) no.10, 104012 [arXiv:1803.10510 [gr-qc]].
- [22] I. D. Saltas and I. Lopes, Phys. Rev. Lett. **123** (2019) no.9, 091103 [arXiv:1909.02552 [astro-ph.CO]].
- [23] E. Babichev, K. Koyama, D. Langlois, R. Saito and J. Sakstein, Class. Quant. Grav. **33** (2016) no.23, 235014 [arXiv:1606.06627 [gr-qc]].
- [24] T. Damour and G. Esposito-Farese, Phys. Rev. Lett. **70**, 2220 (1993).
- [25] T. Damour and G. Esposito-Farese, Phys. Rev. D **54**, 1474 (1996) [gr-qc/9602056].
- [26] T. Harada, Phys. Rev. D **57**, 4802 (1998) [gr-qc/9801049].
- [27] J. Novak, Phys. Rev. D **58**, 064019 (1998) [gr-qc/9806022].
- [28] H. O. Silva, C. F. B. Macedo, E. Berti and L. C. B. Crispino, Class. Quant. Grav. **32**, 145008 (2015) [arXiv:1411.6286 [gr-qc]].

- [29] P. C. C. Freire *et al.*, *Mon. Not. Roy. Astron. Soc.* **423**, 3328 (2012) [arXiv:1205.1450 [astro-ph.GA]].
- [30] L. Shao, N. Sennett, A. Buonanno, M. Kramer and N. Wex, *Phys. Rev. X* **7**, no. 4, 041025 (2017) [arXiv:1704.07561 [gr-qc]].
- [31] A. M. Archibald *et al.*, *Nature* **559**, no. 7712, 73 (2018) [arXiv:1807.02059 [astro-ph.HE]].
- [32] D. Anderson, P. Freire and N. Yunes, *Class. Quant. Grav.* **36**, no. 22, 225009 (2019) [arXiv:1901.00938 [gr-qc]].
- [33] B. Kleihaus, J. Kunz, S. Mojica and E. Radu, *Phys. Rev. D* **93**, 044047 (2016) [arXiv:1511.05513 [gr-qc]].
- [34] D. D. Doneva and S. S. Yazadjiev, *Phys. Rev. Lett.* **120**, 131103 (2018) [arXiv:1711.01187 [gr-qc]].
- [35] H. O. Silva, J. Sakstein, L. Gualtieri, T. P. Sotiriou and E. Berti, *Phys. Rev. Lett.* **120**, 131104 (2018) [arXiv:1711.02080 [gr-qc]].
- [36] G. Antoniou, A. Bakopoulos and P. Kanti, *Phys. Rev. Lett.* **120**, 131102 (2018) [arXiv:1711.03390 [hep-th]].
- [37] G. Antoniou, A. Bakopoulos and P. Kanti, *Phys. Rev. D* **97**, 084037 (2018) [arXiv:1711.07431 [hep-th]].
- [38] M. Minamitsuji and T. Ikeda, *Phys. Rev. D* **99**, 044017 (2019) [arXiv:1812.03551 [gr-qc]].
- [39] P. V. P. Cunha, C. A. R. Herdeiro and E. Radu, *Phys. Rev. Lett.* **123**, 011101 (2019) [arXiv:1904.09997 [gr-qc]].
- [40] I. Z. Stefanov, S. S. Yazadjiev and M. D. Todorov, *Mod. Phys. Lett. A* **23**, 2915 (2008) [arXiv:0708.4141 [gr-qc]].
- [41] C. A. R. Herdeiro, E. Radu, N. Sanchis-Gual and J. A. Font, *Phys. Rev. Lett.* **121**, 101102 (2018) [arXiv:1806.05190 [gr-qc]].
- [42] P. G. S. Fernandes, C. A. R. Herdeiro, A. M. Pombo, E. Radu and N. Sanchis-Gual, *Class. Quant. Grav.* **36**, no. 13, 134002 (2019) [arXiv:1902.05079 [gr-qc]].
- [43] P. G. S. Fernandes, C. A. R. Herdeiro, A. M. Pombo, E. Radu and N. Sanchis-Gual, *Phys. Rev. D* **100**, 084045 (2019) [arXiv:1908.00037 [gr-qc]].
- [44] T. Ikeda, T. Nakamura and M. Minamitsuji, *Phys. Rev. D* **100**, 104014 (2019) [arXiv:1908.09394 [gr-qc]].
- [45] G. Ventagli, A. Lehébel and T. P. Sotiriou, [arXiv:2006.01153 [gr-qc]].
- [46] R. W. Hellings and K. Nordtvedt, *Phys. Rev. D* **7**, 3593 (1973).
- [47] L. Annulli, V. Cardoso and L. Gualtieri, *Phys. Rev. D* **99**, 044038 (2019) [arXiv:1901.02461 [gr-qc]].
- [48] F. M. Ramazanoglu, *Phys. Rev. D* **96**, 064009 (2017) [arXiv:1706.01056 [gr-qc]].
- [49] F. M. Ramazanoglu and K. I. Unluturk, *Phys. Rev. D* **100**, 084026 (2019) [arXiv:1910.02801 [gr-qc]].
- [50] M. V. Ostrogradski, *Mem. Acad. St. Petersburg VI* **4**, **385** (1850).
- [51] R. P. Woodard, *Scholarpedia* **10**, 32243 (2015) [arXiv:1506.02210 [hep-th]].
- [52] L. Heisenberg, *JCAP* **1405**, 015 (2014) [arXiv:1402.7026 [hep-th]].
- [53] G. Tasinato, *JHEP* **1404**, 067 (2014) [arXiv:1402.6450 [hep-th]]; G. Tasinato, *Class. Quant. Grav.* **31**, 225004 (2014) [arXiv:1404.4883 [hep-th]].
- [54] E. Allys, P. Peter and Y. Rodriguez, *JCAP* **1602**, 004 (2016) [arXiv:1511.03101 [hep-th]]; E. Allys, J. P. Beltran Almeida, P. Peter and Y. Rodriguez, *JCAP* **1609**, 026 (2016) [arXiv:1605.08355 [hep-th]].
- [55] J. B. Jimenez and L. Heisenberg, *Phys. Lett. B* **757**, 405 (2016) [arXiv:1602.03410 [hep-th]].
- [56] A. De Felice, L. Heisenberg, R. Kase, S. Mukohyama, S. Tsujikawa and Y. I. Zhang, *JCAP* **1606**, 048 (2016) [arXiv:1603.05806 [gr-qc]].
- [57] A. De Felice, L. Heisenberg, R. Kase, S. Mukohyama, S. Tsujikawa and Y. I. Zhang, *Phys. Rev. D* **94**, 044024 (2016) [arXiv:1605.05066 [gr-qc]].
- [58] A. De Felice, L. Heisenberg and S. Tsujikawa, *Phys. Rev. D* **95**, 123540 (2017) [arXiv:1703.09573 [astro-ph.CO]].
- [59] S. Nakamura, A. De Felice, R. Kase and S. Tsujikawa, *Phys. Rev. D* **99**, 063533 (2019) [arXiv:1811.07541 [astro-ph.CO]].
- [60] A. De Felice, L. Heisenberg, R. Kase, S. Tsujikawa, Y. I. Zhang and G. B. Zhao, *Phys. Rev. D* **93**, 104016 (2016) [arXiv:1602.00371 [gr-qc]].
- [61] S. Nakamura, R. Kase and S. Tsujikawa, *Phys. Rev. D* **96**, 084005 (2017) [arXiv:1707.09194 [gr-qc]].
- [62] J. Chagoya, G. Niz and G. Tasinato, *Class. Quant. Grav.* **33** (2016) no.17, 175007 [arXiv:1602.08697 [hep-th]].
- [63] J. Chagoya, G. Niz and G. Tasinato, *Class. Quant. Grav.* **34** (2017) no.16, 165002 [arXiv:1703.09555 [gr-qc]].
- [64] M. Minamitsuji, *Phys. Rev. D* **94**, 084039 (2016) [arXiv:1607.06278 [gr-qc]].
- [65] L. Heisenberg, R. Kase, M. Minamitsuji and S. Tsujikawa, *Phys. Rev. D* **96**, 084049 (2017) [arXiv:1705.09662 [gr-qc]].
- [66] L. Heisenberg, R. Kase, M. Minamitsuji and S. Tsujikawa, *JCAP* **1708**, 024 (2017) [arXiv:1706.05115 [gr-qc]].
- [67] Z. Y. Fan, *JHEP* **1609**, 039 (2016) [arXiv:1606.00684 [hep-th]].
- [68] A. Cisterna, M. Hassaine, J. Oliva and M. Rinaldi, *Phys. Rev. D* **94**, 104039 (2016). [arXiv:1609.03430 [gr-qc]].
- [69] E. Babichev, C. Charmousis and M. Hassaine, *JHEP* **1705**, 114 (2017) [arXiv:1703.07676 [gr-qc]].
- [70] R. Kase, M. Minamitsuji and S. Tsujikawa, *Phys. Rev. D* **97**, 084009 (2018) [arXiv:1711.08713 [gr-qc]].
- [71] P. Haensel and A. Y. Potekhin, *Astron. Astrophys.* **428**, 191 (2004) [astro-ph/0408324].
- [72] A. Y. Potekhin, A. F. Fantina, N. Chamel, J. M. Pearson and S. Goriely, *Astron. Astrophys.* **560**, A48 (2013) [arXiv:1310.0049 [astro-ph.SR]].
- [73] L. Heisenberg, R. Kase and S. Tsujikawa, *Phys. Lett. B* **760**, 617 (2016) [arXiv:1605.05565 [hep-th]].
- [74] R. Kimura, A. Naruko and D. Yoshida, *JCAP* **1701**, 002 (2017) [arXiv:1608.07066 [gr-qc]].
- [75] R. Brito, V. Cardoso, C. A. R. Herdeiro and E. Radu, *Phys. Lett. B* **752**, 291 (2016) [arXiv:1508.05395 [gr-qc]].
- [76] F. E. Schunck and E. W. Mielke, *Class. Quant. Grav.* **20**, R301 (2003) [arXiv:0801.0307 [astro-ph]].
- [77] R. Kase and S. Tsujikawa, *JCAP* **1308**, 054 (2013) [arXiv:1306.6401 [gr-qc]].
- [78] E. E. Flanagan and T. Hinderer, *Phys. Rev. D* **77**, 021502 (2008) [arXiv:0709.1915 [astro-ph]].
- [79] T. Damour and A. Nagar, *Phys. Rev. D* **80** (2009) 084035 [arXiv:0906.0096 [gr-qc]].
- [80] T. Binnington and E. Poisson, *Phys. Rev. D* **80** (2009) 084018 [arXiv:0906.1366 [gr-qc]].
- [81] T. Hinderer, B. D. Lackey, R. N. Lang and J. S. Read, *Phys. Rev. D* **81**, 123016 (2010) [arXiv:0911.3535 [astro-ph.HE]].

- [82] M. Minamitsuji and H. O. Silva, *Phys. Rev. D* **93**, 124041 (2016) [arXiv:1604.07742 [gr-qc]].
- [83] K. Yagi and N. Yunes, *Science* **341**, 365 (2013) [arXiv:1302.4499 [gr-qc]].
- [84] K. Yagi and N. Yunes, *Phys. Rev. D* **88**, 023009 (2013) [arXiv:1303.1528 [gr-qc]].
- [85] K. Yagi, L. C. Stein, G. Pappas, N. Yunes and T. A. Apostolatos, *Phys. Rev. D* **90**, no. 6, 063010 (2014) [arXiv:1406.7587 [gr-qc]].
- [86] L. C. Stein, K. Yagi and N. Yunes, *Astrophys. J.* **788**, 15 (2014) [arXiv:1312.4532 [gr-qc]].
- [87] C. Breu and L. Rezzolla, *Mon. Not. Roy. Astron. Soc.* **459**, 646 (2016) [arXiv:1601.06083 [gr-qc]].
- [88] D. D. Doneva and G. Pappas, *Astrophys. Space Sci. Libr.* **457**, 737 (2018) [arXiv:1709.08046 [gr-qc]].
- [89] T. Damour and K. Nordtvedt, *Phys. Rev. Lett.* **70**, 2217 (1993).
- [90] T. Damour and K. Nordtvedt, *Phys. Rev. D* **48**, 3436 (1993).
- [91] D. Anderson, N. Yunes and E. Barausse, *Phys. Rev. D* **94**, 104064 (2016) [arXiv:1607.08888 [gr-qc]].
- [92] T. Anson, E. Babichev and S. Ramazanov, *Phys. Rev. D* **100**, 104051 (2019) [arXiv:1905.10393 [gr-qc]].